Vapor Nanobubble-Mediated Photoporation Constitutes a Versatile Intracellular Delivery Technology

Jana Ramon[a], Ranhua Xiong[a], Stefaan C. De Smedt[a], Koen Raemdonck[a] and Kevin Braeckmans[a,*]

[a]Laboratory of General Biochemistry and Physical Pharmacy, Faculty of Pharmaceutical Sciences, Ghent University, Ottergemsesteenweg 460, 9000 Ghent, Belgium

J. Ramon: Jana.Ramon@UGent.be, Dr. R. Xiong: Ranhua.Xiong@Gmail.com, Prof. S. C. De Smedt: Stefaan.DeSmedt@UGent.be, Prof. K. Raemdonck: Koen.Raemdonck@UGent.be

Corresponding author details*
Prof. K. Braeckmans
Email: Kevin.Braeckmans@UGent.be
Tel: +32 9 264 80 98
Fax: +32 9 264 81 89

ABSTRACT

Vapor nanobubble-mediated photoporation has evolved into a promising physical intracellular delivery technology. When irradiated with short but intense laser pulses, photothermal nanomaterials can generate vapor nanobubbles that, when they collapse, induce transient membrane pores through which exogenous effector molecules can be delivered into the cells. Interestingly, this technique offers high-throughput delivery in various cell types, including hard-to-transfect primary cells. A unique feature among cell transfection technologies is its ability to deliver compounds in spatially defined areas, even with single-cell resolution, through controlled scanning of the laser beam. This is especially useful for targeting specific cells in dense heterogenous samples. Although primarily used for permeabilizing the outer cell membrane, this strategy has been exploited to destabilize endosomal and nuclear membranes as well.

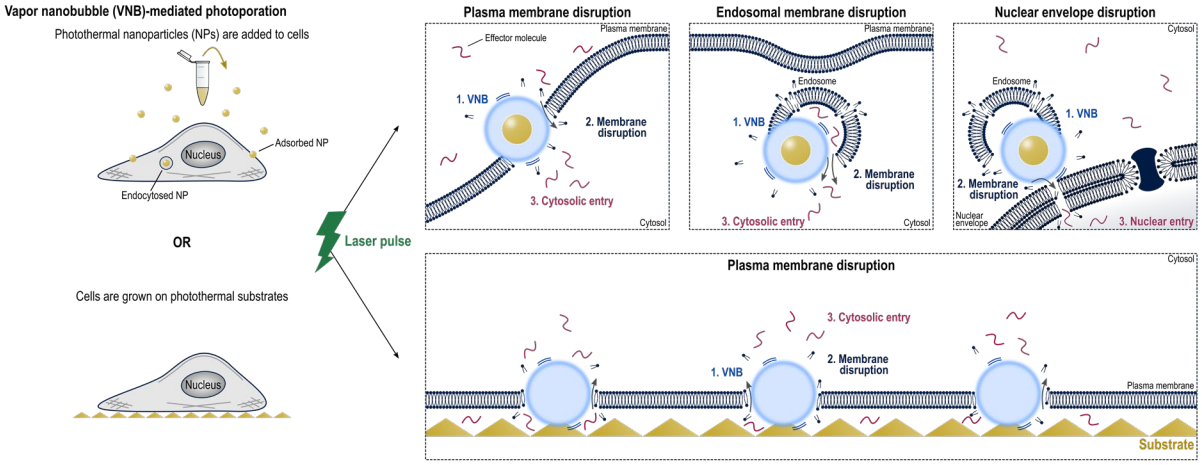

Keywords: Vapor nanobubbles, Photoporation, Laser, Photothermal nanoparticles, Gold nanoparticles, Carbon nanomaterials, Photothermal substrates, Membrane disruption, Intracellular delivery, Cell-selective delivery

1 Introduction

Intracellular delivery of foreign materials into living cells has become indispensable for fundamental biological research as well as a broad range of therapeutic applications, like genome editing and cell-based therapies [1]. For these purposes, most exogenous target molecules like nucleic acids and proteins exhibit unfavorable characteristics (size, charge, stability etc.) impeding spontaneous and efficient crossing of the cell membrane barrier. Over the years, a plethora of delivery strategies ranging from nanocarrier-mediated to membrane disruption-based methods have emerged with the aim of addressing this issue. Nanocarrier-mediated delivery approaches employ bioinspired or synthetic nanomaterials for encapsulation and protection of membrane-impermeable cargo, mostly macromolecules. Nanocarriers can deliver such molecules in cells predominantly by endocytosis or in some cases by direct fusion with the plasma membrane. The most-used bioinspired nanocarriers are viral vectors, which usually offer a high delivery efficiency of nucleic acids by exploiting their viral infection pathways. However, viral vectors are only suited to deliver nucleic acids (of limited size) while their use typically comes with concerns regarding cytotoxicity and immunogenicity. Therefore, it is attractive to look into non-viral synthetic nanocarriers, which are mostly composed of lipids, polymers or inorganic materials [1,2]. Although synthetic nanocarriers are considered to be 'safer', they are often less efficient than their viral counterparts mainly due to poor endosomal escape hampering efficient cytosolic delivery. In addition, the nanocarrier's composition requires optimization per cargo type, which impedes their broad and universal use [3].

Nanocarriers are especially meaningful for *in vivo* drug delivery applications, having the ability to overcome biological barriers and protecting their cargo along their way to target cells in the body. However, when it comes to delivering molecules into cells in an *in vitro* or *ex vivo* setting, a different set of broadly applicable delivery approaches can be used, which are based on the disruption of the cell membrane. Such membrane disruption methods are typically suited to deliver a variety of membrane-impermeable effector molecules into many different cell types [2]. Although some biochemical methods exist to permeabilize the cell membrane, most approaches are of a more physical nature, exploiting mechanical, electrical, thermal or optical stimuli [4]. In strong contrast to nanocarrier-mediated delivery methods, physical membrane disruption delivers exogenous effector molecules directly across the cell membrane and straight into the cell's cytosol. Especially in the past decade, mostly owing to advances in nanotechnology, membrane disruption methods have been perfected for fast, efficient and safe

intracellular delivery *in vitro* or *ex vivo*. A detailed overview of such developments can be found in an extended recent review [1]. Of those emerging technologies, photoporation with nanosensitizers is one of the most flexible ones and will be the focus of this review [5].

Photoporation, also sometimes called optoporation, in its initial form employs a tightly focused high-intensity laser beam to create transient pores in the cell membrane, thereby allowing cytosolic entry of exogenous effector molecules. Although proven useful for single-cell transfections, this approach is inherently slow and labor intensive as only one pore at a time is formed, one cell at a time. Throughput can be tremendously enhanced, however, when combined with photothermal nanomaterials. Such compounds efficiently absorb laser light and convert this energy into photothermal effects that, when in close proximity to the cell membrane, cause transient membrane permeabilization. Because local permeabilization is caused by the photothermal nanomaterials, a tightly focused laser beam is no longer needed and instead a broad (unfocused) laser beam can be used, which can be quickly scanned across the cells, resulting in high-throughput photoporation [5].

A particularly interesting and effective photothermal phenomenon is the generation of water vapor nanobubbles (VNBs), which can emerge from laser-irradiated photothermal nanomaterials in a hydrated environment. In its most straightforward form, VNB-mediated photoporation is performed through the use of photothermal nanoparticles (NPs) that are supplemented to cells in culture. As illustrated in **Figure 1**, once added to the cells, these NPs will interact with the cell membrane, usually either through electrostatic interaction or high-affinity ligand-receptor coupling. Typically, after a certain incubation time, unbound NPs are removed through a washing step and cells are subjected to laser treatment. VNB generation is usually achieved with intense laser pulses with a duration of less than 10 ns. By delivering the laser energy on such a short time scale, heat has no time to diffuse out, which causes the particle's temperature to increase quickly by several hundreds of degrees. Water in contact with the NP will quickly evaporate, resulting in a fast expanding VNB that emerges around the NP's surface. When the thermal energy of the NP is consumed, the VNB collapses. Emitted pressure waves combined with shear stress from fluid streams can subsequently impose significant mechanical stress to a nearby cell membrane, thus eventually causing very localized pore formation in a spatiotemporally controlled manner with negligible heating of the environment [6–8]. Apart from passive diffusion through the created pores, Lukianova-Hleb et al. also suggested that fluid jets provoked upon bubble collapse can boost intracellular delivery by active hydrodynamic injection of effector molecules through the pores [9]. Additionally, it has

been shown that VNBs, under certain conditions, can be generated by a non-thermal plasma-mediated mechanism, as will be discussed later on (**Section 2.2**) [10,11].

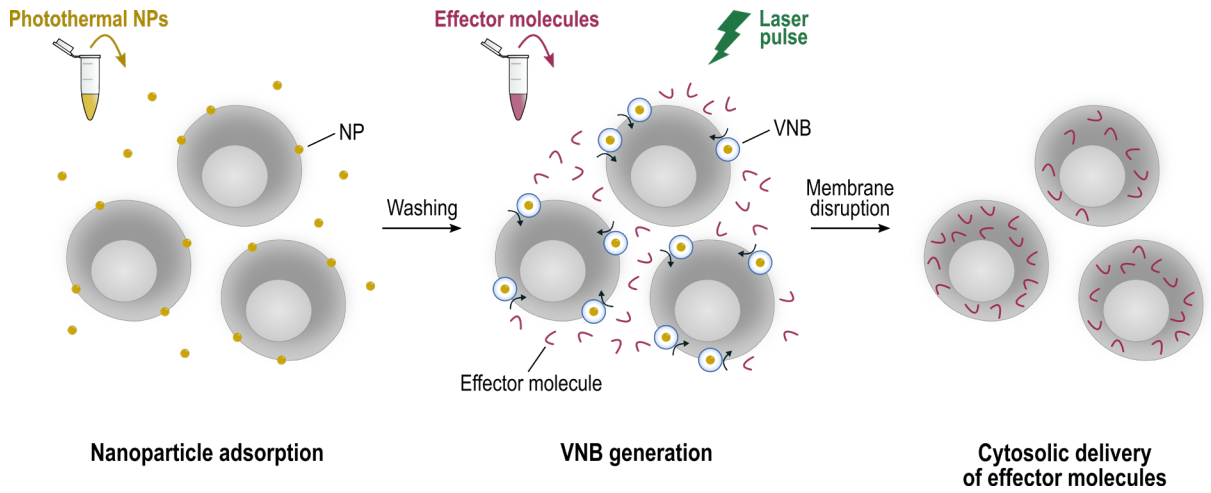

Figure 1. Schematic overview of the most commonly used photoporation protocol. Once added to the cells, photothermal NPs will adsorb to the cell membrane. After washing away free NPs, cells are irradiated with pulsed laser light. This results in the formation of a VNB, emerging from the particle's surface through evaporation of the surrounding water. Upon VNB collapse, nearby cell membranes are disrupted through mechanical effects, such as pressure waves and fluid shear forces. Finally, exogenous effector molecules are able to diffuse into the cell's cytosol through the transient pores. NP, nanoparticle; VNB, vapor nanobubble.

Cell membranes can be permeabilized to some extent by mere heating of the NPs as well, which is what happens predominantly when continuous wave (CW) laser irradiation or low-intensity laser pulses are applied. However, for the typically used 60-70 nm gold NPs (AuNPs), this effect was shown to be less efficient than permeabilization by VNBs, especially for larger macromolecules [7]. Being a universal physical membrane disruption technique, VNB-mediated photoporation has been demonstrated to promote highly efficient intracellular delivery in both adherent and suspension cells [8,9,12–14]. Furthermore, by tuning the laser diameter to match the size of the cells, highly selective single-cell delivery is possible as well [15].

This review will focus on VNB-mediated photoporation for the intracellular delivery of membrane-impermeable effector molecules thereby highlighting recent advances in the field. First, a more in-depth explanation will be given of the principles behind laser-induced VNBs, followed by types of photothermal nanomaterials that have been used for this purpose. Both photothermal NPs in solution and photothermal substrates will be discussed. Next, we will

124 elaborate on pore-forming mechanisms and how cells respond to and repair membrane damage.
125 Furthermore, the cell-selective targeting potential of VNB-mediated photoporation will be
126 highlighted. Finally, an overview of recent advances in intracellular delivery by VNB-mediated
127 photoporation will be given, with special attention to the types of effector molecules that have
128 been delivered and the different types of cells to which it was successfully applied. Although
129 primarily used for permeabilizing the outer cell membrane, this section will also cover
130 applications involving destabilization of endosomal and nuclear membranes.

131 2 Laser-induced vapor nanobubble formation: fundamentals, mechanisms and 132 characteristics

133 Throughout the last decade, the use of photothermal NPs for photoporation has become
134 increasingly important as they allow to improve the precision and throughput of the
135 photoporation procedure tremendously. Considering their unique optical features, plasmonic
136 NPs, mostly AuNPs, have up until now extensively been used for this purpose. Other
137 photothermal nanomaterials like carbon-based (carbon black, graphene, etc.) NPs and metallic
138 titanium nanostructures have been used as well. VNBs incited by pulsed laser irradiation of
139 such nanomaterials are mostly formed through thermal mechanisms, although a non-thermal
140 plasma-mediated process has been described as well. Both mechanisms, correlated with their
141 optical parameters, will be discussed in this section. Note that the description here will focus
142 on NPs in solution, but mechanisms are also applicable when nanomaterials are integrated in
143 photothermal substrates or other kinds of devices.

144 *2.1 Thermal-induced vapor nanobubbles*

145 2.1.1 Thermalization of nanoparticles

146 When irradiated with laser light, photothermal NPs have the unique ability to absorb the
147 laser energy and convert it to heat, a process that is referred to as NP thermalization. Of course,
148 an important requirement is that the spectrum of the incident light matches the NP's absorption
149 spectrum. For plasmonic NPs, like AuNPs, light absorption is significantly enhanced by their
150 localized surface plasmon resonance (LSPR), as illustrated in **Figure 2A**. Upon irradiation of
151 such NPs, their free electrons are forced to move in reaction to the oscillating electrical
152 component of the incident electro-magnetic wave. The net movement of free electrons to one
153 side of the NP causes its opposite side to attain a net positive charge stemming from the
154 remaining lattice ions. This results in an induced electrical dipole, wanting to drive the electrons

back to equilibrium. The combination of the driving force from the oscillating electric field and the restorative force from the induced dipole results in an oscillatory movement of the free electrons, which are called localized surface plasmons, with a certain amplitude. Depending on the NP's composition, size, shape and local environment, the amplitude of the localized surface plasmons will be maximal for certain wavelengths, a property that is referred to as resonance. Therefore, the absorption spectrum of plasmonic NPs is very much dominated by an absorption peak over a narrow range of wavelengths at which light energy is maximally transferred to the NPs, linked with the phenomenon of LSPR [5,16,17]. Solid gold nanospheres, for instance, have an LSPR peak in the visible range [17,18], whereas gold nanorods [19,20], core-shell NPs [21] and gold nanostars [22] show a distinct plasmon peak in the near-infrared (NIR) region.

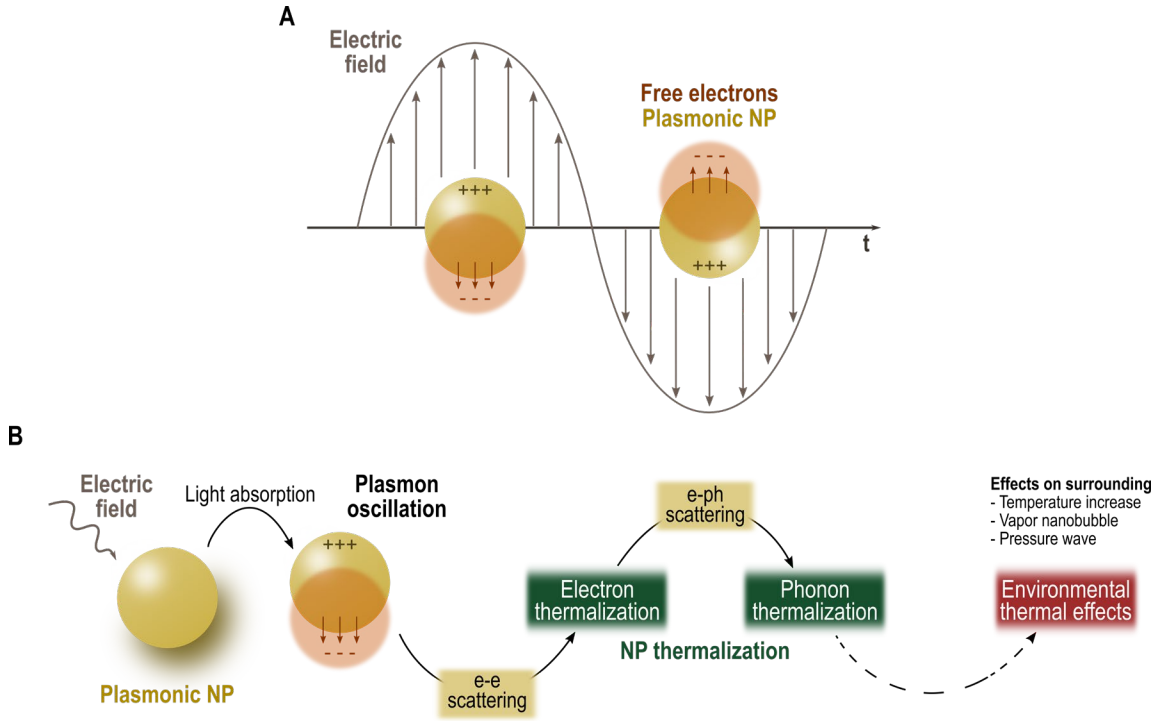

Figure 2. LSPR and corresponding energy transfers upon interaction of a plasmonic NP with an electric field. **A.** The incident laser light causes charge separation in the plasmonic NP, which subsequently induces an electrical dipole driving the electrons back to equilibrium. The combination of both forces results in oscillation of the localized surface plasmons (free electron cloud) with a certain amplitude. Upon irradiation at the NP's resonant wavelength, the light energy is maximally transferred to the NP whose plasmons will oscillate with maximal amplitude. **B.** Schematic overview of the energy cascade within a NP upon plasmon oscillation. E-e, electron-electron; e-ph, electron-phonon; NP, nanoparticle.

As illustrated in **Figure 2B**, LSPR is followed by a cascade of energy transfers within the plasmonic NP. Oscillating electrons first become thermalized through electron-electron scattering after which they will transfer their energy to the lattice, which in turn becomes thermalized via electron-phonon scattering. In general, thermal equilibration in an NP typically occurs within 100 ps upon laser irradiation, after which heat can be transferred to the local surrounding medium [5,17].

2.1.2 Vapor nanobubble nucleation

Upon laser-induced heating of a photothermal NP, energy of the thermalized NP can dissipate to the local environment. This may increase the temperature of the surrounding medium and even result in the formation of a thermal-induced VNB if the NP's temperature exceeds the medium's critical temperature (**Figure 3**) [6,23]. In the latter case, a thin nanometer-sized vapor layer, referred to as the VNB nucleus, will emerge and start to expand with a bubble size mounting up to a few hundred nanometers depending on the available energy and size of the NP. When the thermal energy of the NP is consumed, the VNB subsequently collapses, which typically occurs 10 to 100 ns after the onset of nucleation [6,7,24]. Even though heating is at the origin of this phenomenon, a peculiar feature is that virtually no heat is further transferred to the surroundings upon VNB formation. This can be explained by the relative insulating nature of a gas combined with the very short bubble lifetime (<μs). As a result, almost all thermal energy is converted to mechanical energy of the expanding and collapsing VNB [6,23].

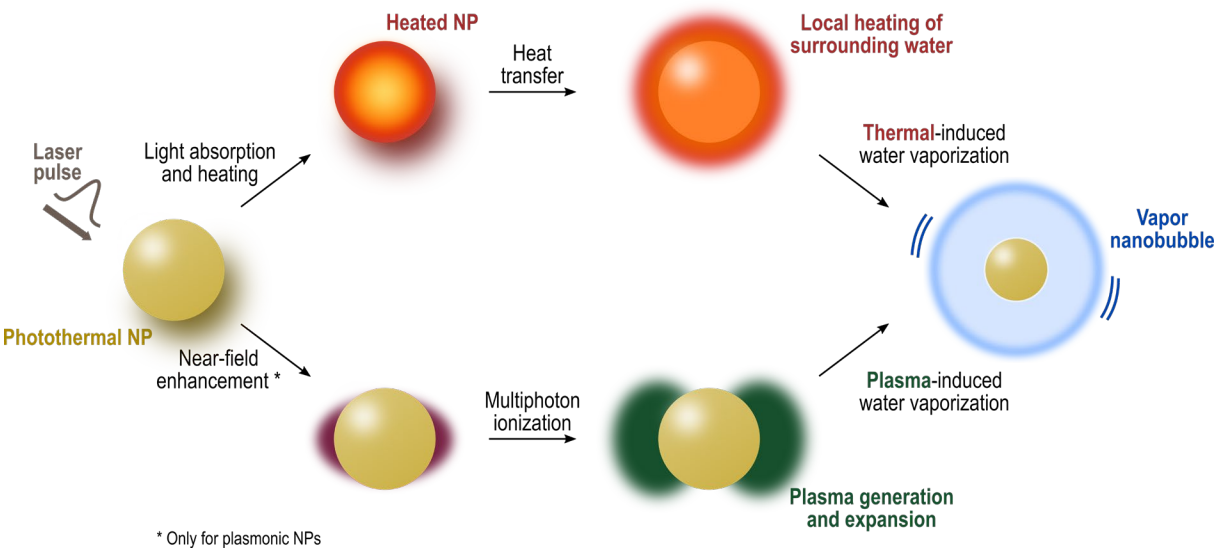

Figure 3. VNB nucleation mechanisms around a photothermal NP. A VNB can either be thermally induced or plasma induced. The former relies on the extreme heating of the NP lattice whereas the latter is provoked by plasma generation in the near field. NP, nanoparticle.

Typically, pulsed laser light (<10 ns) is used for VNB nucleation as this laser mode delivers a sufficient amount of light energy within a short enough time for the required extreme and rapid NP heating [6,7,23]. In contrast, when longer laser pulses or even CW laser irradiation are used, thermal energy can already start to diffuse out of the NP before all light energy is delivered, in which case there is less chance that the NP's temperature will reach the critical temperature of the surrounding liquid. Such type of laser irradiation does not confine heating of the NP in time and space and will usually result in heating of the environment rather than the generation of VNBs [25,26]. Still, it should be mentioned that large micro-scale to macro-scale vapor bubbles have been reported upon high-intensity CW laser irradiation of large microscopically visible AuNP clusters, although these originated from the extreme bulk heating of the environment [27].

The VNB generation threshold, typically defined as the minimal laser fluence level (J/cm^2) at which 90% of the irradiated NPs form VNBs, is inversely correlated with the pulse duration and will also strongly depend on the type of NP (**Section 3.1**) [6]. The Lapotko group, in particular, has thoroughly investigated thermal-induced VNBs from AuNPs. As thermal equilibration of the NP lattice already occurs within 100 ps after laser irradiation, it was found that picosecond pulses are more efficient for VNB formation (i.e., require a lower laser fluence) compared to nanosecond pulses [6,23,27]. The same goes for even shorter femtosecond laser pulses as others have pointed out [17]. These observations can be explained by the fact that a VNB already starts to form after a few hundreds of picoseconds and thereby 'shields' the NP from the remainder of the laser pulse that is still to arrive. More specifically, for laser pulses much longer than 100 ps, only a part of the laser light is effectively used for VNB formation as the rest will become partly scattered and hence does not contribute as efficiently to further NP heating [23,27]. Nevertheless, in practice, nanosecond laser pulses have been used the most as such lasers are available with high powers at only a fraction of the cost compared to femtosecond or picosecond lasers.

2.2 Plasma-induced vapor nanobubbles

For plasmonic nanomaterials, high-intensity femtosecond laser pulses can generate VNBs via a non-thermal mechanism. LSPR, described under **Section 2.1.1**, induces near-field

227 enhancement of the electric field around the NP's edges with an intensity that is dependent on
228 the particle size and geometry [17,18]. As illustrated in **Figure 3**, by multiphoton ionization of
229 water molecules in this near-field region and ejection of electrons from the NP, a local plasma
230 of charged particles (i.e., electrons and ions) can be generated. The plasma subsequently
231 diffuses and recombines with water molecules whose thermal energy increase, eventually
232 leading to VNB formation around the NP. Plasma-induced VNBs have been shown to prevail
233 when off-resonant femtosecond laser pulses are used, that is with a wavelength outside of the
234 LSPR peak. Instead, when irradiated within the LSPR peak, it is the thermal induction of VNBs
235 that will dominate [10,11,17]. However, the boundary between thermal- and plasma-induced
236 VNBs is rather thin with a sudden transition between both mechanisms depending on
237 experimental parameters. This was clearly demonstrated by Boulais et al. who used in-resonant
238 femtosecond laser irradiation of gold nanorods and reported shifting of the absorption regime
239 (thermal-induced VNBs) toward the near-field regime (plasma-induced VNBs) when
240 increasing the laser fluence above a certain level [19].

241 Meunier and colleagues were the first to study plasma-induced VNBs from AuNPs using
242 off-resonant femtosecond laser pulses, pointing out some clear advantages over the thermal-
243 induced VNB mechanism. They demonstrated that overheating of AuNPs did not take place
244 thereby avoiding particle destruction. In addition, the possibility to use NIR wavelengths is
245 beneficial for biological applications due to better tissue penetration and less tissue damage
246 compared to visible light [10,11,28]. On the other hand, femtosecond laser set-ups are much
247 more expensive and complicated to operate compared to nanosecond lasers. Hence, combined
248 with the availability of NIR-absorbing NPs, this is likely the primary reason why nanosecond
249 lasers and thermal-induced VNBs are still explored the most to date.

250 3 Photothermal nanomaterials and substrates for vapor nanobubble-mediated 251 photoporation

252 To permeabilize cells by laser-induced VNBs, two modalities have been proposed. The
253 first and most-used approach is incubation of cells with photothermal NPs that can interact with
254 the cell membrane and create pores upon laser-induced VNB formation. A second approach
255 involves the design of photothermal substrates on which cells can be cultured and which can
256 form laser-induced VNBs at distinct places where cells are in contact with the substrate. Both
257 approaches will be described in this section.

258 *3.1 Photothermal nanoparticles*

So far, AuNPs have been used the most as photothermal enhancers for VNB-mediated photoporation. By tailoring their size and structure, their plasmon peak can be adjusted over the visible to NIR range. Typically, solid gold nanospheres display an LSPR peak in the visible region, which can be more or less tuned toward shorter or longer wavelengths by decreasing or increasing their size, respectively [17,18]. Shifting of the absorption spectrum further to the NIR region is possible by allowing the NPs to aggregate, thus effectively forming larger gold clusters that optically behave as single particles due to plasmon coupling between the individual NPs. For instance, Lukianova-Hleb et al. demonstrated that endosomal clustering of 60 nm antibody-functionalized AuNPs rendered large enough sizes for thermal-induced VNB formation when irradiated with 780 nm picosecond laser pulses [29]. Furthermore, in earlier studies, the same group also reported that clustered NPs (irrespective of the particle geometry) can provoke thermal-induced VNBs at a lower threshold than the individual NPs, which can be explained by the synergistic effect of the larger size (i.e., lower Laplace pressure) and the joint contribution of the individual particles to VNB nucleation [6,23]. Importantly, increasing size does not infinitely correlate with a lower VNB generation threshold. Lukianova-Hleb et al. reported that for solid gold nanospheres, a size of 80 nm was most efficient for bubble formation as further increasing the size to 250 nm resulted in a 1.3-fold increase of the VNB generation threshold [6]. This can be explained by the higher heat capacity, which is proportional to the gold nanosphere's volume. Other shapes and configurations like nanorods, core-shell NPs and nanostars show a distinct plasmon peak in the NIR region as well, which makes them especially attractive for *in vivo* applications [19–22,30]. Interestingly, these types of configurations may also have a lower VNB generation threshold compared to solid gold nanospheres [6,23]. Given their potential to control laser-induced damage, efforts are being made to further optimize these structures by downsizing their optimal VNB generation threshold. For instance, Santra et al. recently developed nano-corrugated mushroom-shaped gold-coated polystyrene NPs that, linked with their highly corrugated surface, are expected to generate thermal-induced VNBs at a lower laser fluence than spherical core-shell NPs, based on theoretical considerations [21]. This theoretical difference in VNB generation potential between both types of core-shell NPs can be explained by the electromagnetic near-field enhancement around the nano-corrugated edges, which creates local heating hotspots, thus facilitating VNB nucleation.

Side effects of such rapid and excessive heat formation, as needed for thermal-induced VNB formation, include alteration and even destruction of the AuNPs. This has been profoundly studied for different types of AuNPs and involves melting, surface evaporation and

292 fragmentation of the nanomaterial when laser-induced temperatures exceed melting and
293 evaporation thresholds. Fragmentation of AuNPs changes their optical properties because
294 LSPR is size dependent. Typically, smaller-sized fragments are not able to induce VNBs under
295 the same conditions due to narrowing and shifting of the plasmon peak toward shorter
296 wavelengths [18,30]. As a consequence, AuNPs can typically only be used once to form
297 thermal-induced VNBs after which they are destroyed [31]. Nevertheless, repeated bubble
298 formation around AuNP clusters with multiple laser pulses has been reported by the Lapotko
299 group [23,32]. As a possible explanation it was proposed that not all NPs in the cluster were
300 destroyed upon pulsed laser irradiation. Also Teirlinck et al. observed repeated VNB formation
301 from AuNPs that were dispersed in a bacterial biofilm [33]. The authors hypothesized that this
302 effect could be due to re-aggregation of smaller AuNP fragments in the biofilm matrix, which
303 act as newly assembled NPs. Besides size reduction, reshaping of gold nanorods to nanospheres,
304 even at temperatures much lower than the melting temperature, has also been reported, resulting
305 in a shift of the LSPR peak from the NIR to the visible spectrum [19]. Together this shows that,
306 under conditions for thermal-induced VNBs, AuNPs are likely to become altered or destroyed
307 upon laser activation, thus losing their original optical properties thereby hampering repeated
308 VNB formation. To tackle these thermal instability issues, alternative nanostructures, discussed
309 hereunder, are being investigated as possible sensitizers for VNB-mediated photoporation.
310 Another solution can be to switch to plasma-induced VNBs, induced by off-resonant
311 femtosecond laser irradiation, as discussed under **Section 2.2**.

312 Carbon-based materials like carbon black and graphene NPs have proven to be valuable
313 alternatives to AuNPs, which is predominantly linked with their enhanced thermal stability. As
314 first reported by the Prausnitz group, carbon black NPs mixed with (detached) cells in
315 suspension were shown to offer efficient intracellular delivery of different macromolecules
316 when irradiated with in-resonant femtosecond to nanosecond NIR laser pulses [34,35]. In their
317 protocol, unbound NPs are not washed away before laser irradiation, even though they noticed
318 that membrane disruption was most likely induced by NPs in close proximity to the plasma
319 membrane [36]. The authors hypothesized that permeabilization was caused by photoacoustic
320 forces that arise from the carbon-steam reaction (i.e., chemical reaction between water and
321 carbon), although they stated that thermal or other factors, such as perhaps thermal-induced
322 VNBs, may have contributed as well [34–36]. Studies by Jumelle et al. explored femtosecond
323 laser activation (150 fs, λ=800 nm) of carbon nanoparticles via an adapted protocol, which
324 avoids a cell detaching step before laser irradiation [37,38]. The authors demonstrated

successful delivery of calcein and dextran macromolecules, respectively in a monolayer of human corneal endothelial cells [37] and *ex vivo* in the intact endothelium of whole human corneas [38]. Although not proven, membrane disruption and intracellular delivery was attributed to bubble formation following the carbon-steam reaction. In a recent study from the Prausnitz group, carbon nanotubes (single-walled and multi-walled) were evaluated as nanosensitizers of which it was noticed that they had a different photoporation behavior compared to the previously studied carbon black NPs [39]. With increasing laser fluence, intracellular delivery, cell toxicity and cell fragmentation increased for carbon black NPs. In contrast, for single-walled carbon nanotubes, all three parameters remained low for all laser fluences whereas for multi-walled carbon nanotubes, no clear correlation between cell death and laser fluence was observed, as cells were either alive or fragmented. Of note, given the rise in photoacoustic pressure around the laser-irradiated NPs, the authors assumed the involvement of thermal-induced VNBs. Around the same time it was demonstrated by our group that other carbon-based nanomaterials can be used as well, like graphene quantum dots (GQDs) and reduced graphene oxide (rGO) [13,31]. In particular, it was demonstrated that multiple thermal-induced VNBs could be formed up to 4 times from GQDs upon sequential nanosecond pulsed laser irradiation, while 70 nm AuNPs fragmented already after the first laser pulse [31]. In a follow-up, study it was shown that cell viability could be improved by coating GQDs and rGO with polyethylene glycol (PEG) and polyethylenimine (PEI), which resulted in enhanced colloidal stability and more uniform VNB formation upon addition to cell cultures [13]. In addition, it was demonstrated that rGO is compatible with NIR irradiation, resulting in successful intracellular fluorescein isothiocyanate (FITC)-dextran delivery with 800 nm picosecond pulses.

Because of the very localized action of VNBs, association of photothermal NPs to the cell membrane seems to be an important requirement for effective permeabilization. The most straightforward way to achieve this is by electrostatic interaction of NPs with the negatively charged cell membrane. A cationic charge is conferred to NPs by coating them with positively charged polymers. Ammonium polymers, like poly(diallyl dimethyl ammonium chloride), have been used in the context of photoporation to provide NPs with a net positive charge that is independent of the pH [14,40–42]. And also PEI has been successfully applied for this [13]. Furthermore, functionalization with cationic polymers enhances colloidal stability as is also attained with PEG [13,21,43] and surfactants like sodium dodecyl sulfate [34] and Polysorbate [35] that, however, do not improve electrostatic interaction with the cell membrane. Apart from

358 (unspecific) electrostatic interactions, one can also opt to functionalize the NPs with a ligand,
359 such as an antibody, targeted toward a specific cell membrane receptor. This has been
360 extensively studied by Yao et al. who demonstrated superior cell binding of antibody-
361 functionalized AuNPs compared to their non-functionalized counterparts, thereby enhancing
362 intracellular delivery [20,44,45]. Furthermore, targeted binding of the photothermal NPs to cell-
363 specific receptors offers the advantage that a particular cell type can be treated selectively while
364 being in the presence of other cell types (**Section 5.2**) [9,29,46,47].

365 A detailed overview of NPs and their characteristics (material, morphology, size, surface
366 functionalization, clustering) as well as their use in cytosolic delivery via plasma membrane
367 disruption, linked with laser parameters, reported delivery efficiency and cell viability is given
368 in **Table 1**.

369 *3.2 Photothermal substrates*

370 Instead of photothermal NPs, it is also possible to incorporate photothermal features into
371 substrates from which thermal-induced VNBs can nucleate upon pulsed laser irradiation. Not
372 surprisingly, such substrates have hence been used as well for cell culture and subsequent VNB-
373 induced permeabilization of cells in contact with the substrate. Early on, Wu et al. developed
374 the biophotonic laser-assisted surgery tool (BLAST) (**Figure 4A**) [48]. This set-up consists of
375 a silicon chip covered with a thin, micrometer-wide porous SiO_2 membrane whose trans-
376 membrane holes are asymmetrically coated with crescent-shaped titanium thin films.
377 Microcavitation bubbles nucleate from the intense heating of the metallic titanium thin film,
378 resulting in transient pore formation of cell membranes adhered to the silicon chip. Intracellular
379 delivery, in this case, is substantially enhanced by pressure-driven flow through vertical silicon
380 channels mounted underneath the fragile silicon membrane. The authors reported high-
381 throughput (100 000 cells/min) delivery of bacteria, enzymes, and NPs in several cell types.
382 Madrid et al. fabricated a silica nanocavity substrate coated with a thin titanium film through a
383 self-assembly process that allows for fairly easy manufacturing of the substrate (**Figure 4B**)
384 [49]. Upon 11 ns 1064 nm pulsed laser irradiation, extreme and rapid heating followed by the
385 generation of cavitation bubbles was reported, which led to intracellular delivery of calcein
386 (~78% positive cells) at a throughput of 30 000 cells/min and a cell viability of ~87%, as
387 determined by microscopy analysis of Calcein AM live-cell staining. In earlier work from the
388 same group, Saklayen et al. developed pyramidal nanoheaters covered with a thin gold film
389 that, under identical laser conditions, strongly localized laser energy and heating toward the

apex of each pyramid (**Figure 4C**) [50]. The generated hotspots eventually triggered the formation of thermal-induced VNBs, which led to permeabilization of cells cultured on top of the pyramids. Interestingly, in contrast to AuNPs, no visible damage to the nanostructure was observed at the optimal laser fluence of 54 mJ/cm². The authors reported reproducible intracellular delivery of a wide range of molecules (~95% positive cells for 0.6 kDa, the smallest molecule tested) with high cell viability (~98%), as determined via microscopy analysis and flow cytometry measurements with Calcein AM live-cell staining. This was achieved with a throughput of 50 000 cells/min. In another study, Raun et al. used a similar set-up but replaced gold by a thin titanium nitride coating thereby presenting a higher melting temperature, which could render improved stability of the film over time [51]. A recent study by Zhao et al. reported a large plasmonic array with gold square-shaped 'nanodisks', demonstrating again that, after 6 ns 532 nm laser pulses, thermal-induced VNBs are formed at the plasmonic hotspots, this time situated at the corners of each nanodisk (**Figure 4D**) [52]. The authors reported comparable delivery efficiency, cell viability and scanning speed as for the plasmonic pyramidal nanoheaters from Saklayen et al. In this case, cell viability was determined by microscopy analysis of dead cells stained with propidium iodide (PI). Optimal laser fluence, however, was a factor 5 lower (~11 mJ/cm²), which may be attributed to the generation of multiple hotspots at the nanodisk edges rather than a single one at the pyramid tip.

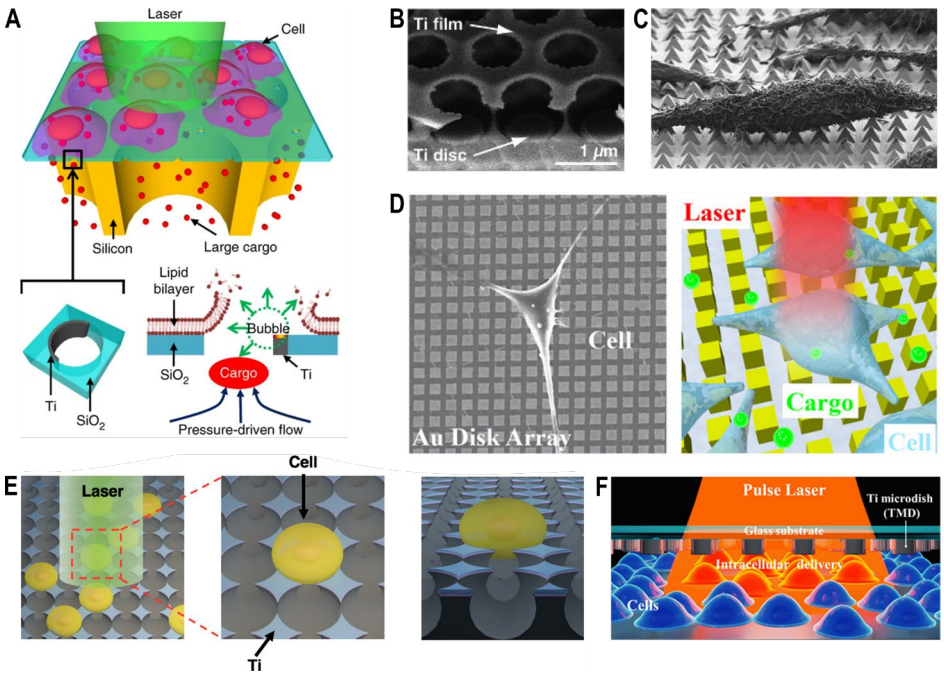

Figure 4. Overview of photothermal substrates used for VNB-mediated photoporation. **A.** The BLAST. Reproduced with permission from [48]. Copyright 2015 Springer Nature. **B.** A self-

assembled thermoplasmonic silica nanocavity substrate coated with a thin titanium film. Reproduced with permission from [49]. Copyright 2018 American Chemical Society. **C**. Pyramidal nanoheaters covered with a thin gold film. Reproduced with permission from [50]. Copyright 2017 American Chemical Society. **D.** A plasmonic gold nanodisk array. Reproduced with permission from [52]. Copyright 2020 American Chemical Society. **E.** Sharp titanium-coated tips embedded in microwells for trapping of suspension cells. Reproduced with permission from [53]. Copyright 2019 American Chemical Society. **F.** Titanium microdish device. Reproduced with permission from [54]. Copyright 2020 American Chemical Society.

The photothermal substrates mentioned so far rely on close contact of the cells at the photothermal hotspots. As such they are most suited for adherent cells, and less for suspension cells. Man et al., however, developed a delivery platform for suspension cells consisting of microwells with sharp nanoscale titanium-coated tips positioned at the edge of the wells, which can form hotspots upon pulsed laser irradiation (**Figure 4E**) [53]. Owing to its design, suspension cells can be trapped via gravity-assisted self-alignment within the microwells. Efficient delivery into Ramos B cells was reported for a broad range of molecule sizes (>84% for 0.6 kDa, the smallest molecule tested) upon 6 ns 532 nm pulsed laser irradiation with a throughput >100 000 cells/min. This was accompanied by a cell viability >96%, as assessed by microscopy analysis of dead cells stained with PI. Another recently developed technique by Shinde et al. involves titanium microdishes (3 µm) mounted onto a larger chip substrate (**Figure 4F**) [54]. The device is aligned on top of the cell layer in such a way that it is close enough to induce membrane perforation but at the same time precludes contact with the cells. Although not actually demonstrated, thermal-induced VNBs were also considered to be involved in the membrane perforation mechanism as temperature simulations implied that the water surrounding the microdishes exceeded the critical temperature necessary for cavitation processes. Together these studies prove that nanoplasmonic arrays are a useful concept to permeabilize cells with laser-induced VNBs. Widespread use is, however, limited at present considering the need for dedicated cleanroom microfabrication techniques. It also remains unclear to which extent culturing cells on (sharp) microscale protrusions may have an effect on their normal functioning.

4 Cell response to vapor nanobubble-mediated membrane disruption

Following pore formation in the cell membrane, including by laser-induced VNBs, the balance of osmolytes between the intracellular and extracellular milieu becomes disturbed (e.g.

443 outflux of potassium and influx of calcium), which will activate stress responses and membrane
444 repair mechanisms [1,55]. Fast plasma membrane resealing will already occur within minutes
445 after membrane disruption through a variety of mechanisms, including contraction, patching,
446 plugging, exocytosis, internalization and externalization through endocytosis and shedding,
447 respectively. Although those mechanisms are still under investigation, they likely depend on
448 the pore size, cell type and environmental conditions [56]. When membrane perturbation is
449 extreme, initial cell repair mechanisms may be insufficient in rapidly restoring membrane
450 integrity, leading to cell death. Even when membrane repair is successful, cells may suffer from
451 osmotic stress, inevitably leading to cell swelling and ultimately necrotic cell death [57]. This
452 does not necessarily mean that cells that have avoided such faith are completely unaffected.
453 Once the plasma membrane is resealed, secondary responses are triggered to restore, for
454 example, ATP, potassium and calcium levels [1]. In parallel, the cell will also try to repair
455 damage to its cytoskeleton [58]. Importantly, restoring the cell's homeostatic balance and
456 functionality can take several hours or even days, which is notably longer than the fast initial
457 membrane resealing response. When elevated stress levels are present for extended periods of
458 time, cells are at risk of obtaining permanent alterations (e.g. fate changes, loss of potency and
459 mutations) or can eventually undergo programmed cell death like apoptosis [1,59].

460 When subjecting cells to VNB-mediated photoporation, treatment conditions need to be
461 fine-tuned so as to minimize the extent of cell toxicity while maximizing intracellular delivery
462 efficiency of the effector molecules. Parameters that are typically optimized for a given
463 combination of cell type and effector molecule are the concentration of NPs, their cell
464 incubation time and laser fluence. Cell toxicity, correlated with each of these conditions, can
465 be monitored in a variety of ways. The fraction of dead cells can be determined using live/dead
466 staining, such as markers leaking from cells (e.g. Calcein AM) when cell membrane integrity
467 is lost and/or fluorescent DNA binding dyes (e.g. PI) unable to penetrate intact cells. As a word
468 of caution we would like to note that quantification of cell viability is in many studies done by
469 flow cytometry [12,20,34,43,60,61]. However, this easily leads to an underestimation of the
470 number of dead cells since highly fragmented cells, which end up in debris background are not
471 accounted for, apart from the fact that dead cells are also easily removed by washing steps. It
472 is therefore insufficient to quantify cell viability by flow cytometry with live/dead staining
473 alone. Ideally, these strategies should be accompanied by more robust methods, such as cell
474 counting or metabolic assays like the MTT or CellTiter-Glo® assay, which present a better view
475 of what happens to the entire cell population [8,28,35,62]. Studies in which cell viability

476 investigations are only based on live/dead staining with flow cytometry analysis are, therefore,
477 indicated in **Table 1** because the reported cell viability values should be interpreted with this
478 cautionary note in mind.

479 As noted above, even if cells survive and are designated as 'viable' according to the
480 above-mentioned assays, prolonged elevated stress levels can cause alterations in a cell's
481 homeostasis and normal functioning. For instance, a recent study by Raes et al. compared the
482 proliferating potential of Jurkat T cells treated either by electroporation or VNB-mediated
483 photoporation [14]. They found that the 'viable' electroporated cells suffered from a complete
484 loss of cell-proliferative potential even 5 days after treatment, whereas for photoporated cells
485 this was not the case. Loss of function and phenotypic changes of electroporated T cells have
486 been pointed out by others as well [63]. Altogether, these observations point toward the
487 importance to progress beyond measuring short-term acute toxicity and instead also monitor
488 cell health at longer time scales. This is particularly important when a delivery technique is
489 used in the context of cell-based therapies where cell functionality needs to be guaranteed once
490 administered to the patient. An example in the context of VNB-mediated photoporation is the
491 study by Fraire et al. who performed whole transcriptome analysis covering both short-term
492 and long-term effects on cell homeostasis [42]. The authors, in this case, exploited 95 nm
493 cationic AuNPs as carriers for small interfering RNA (siRNA). After endocytosis of the siRNA-
494 functionalized AuNPs in HeLa cervical cancer cells, pulsed laser irradiation was applied to
495 destabilize endosomal membranes by photothermal heating or VNB formation. They reported
496 that, for both laser regimes, DNA repair pathways were not upregulated, nor did they see
497 alterations in programmed cell death pathways like apoptosis or necroptosis. Although this
498 study paves the way toward more in-depth knowledge regarding VNB-induced interaction of
499 photothermal nanomaterials with cells, this is only the tip of the iceberg. Further research is
500 necessary to fully map poration-induced changes and cell functionality effects over a longer
501 period of time and in relevant cell types.

502 5 Vapor nanobubble-mediated photoporation of selected cells

503 *5.1 Laser beam targeting*

504 A unique feature of (VNB-mediated) photoporation, compared to other physical
505 membrane disruption techniques, is that it can permeabilize cells in a spatially controlled
506 manner by proper scanning of the laser beam. Fast spatial-selective intracellular delivery by
507 VNB-mediated photoporation using 70 nm cationic AuNPs was demonstrated by Xiong et al.,

who dubbed this principle spatially resolved nanoparticle-enhanced photoporation (SNAP) [15]. By scanning of the laser beam, compounds were delivered into cell cultures according to intricate pre-defined patterns. Although the authors used a fairly slow 20 Hz nanosecond pulsed laser (7 ns, λ=561 nm), still a respectable photoporation rate of ~10 000 cells/min was reached. In addition, by tuning the laser beam diameter to the size of individual cells, they demonstrated the possibility of targeting single cells, which were either manually selected or identified by (automated) image processing. Going beyond a mere technical proof-of-concept demonstration, image-guided SNAP of cells was successfully applied to selectively deliver a contrast agent in polynuclear normal human epidermal keratinocytes, which is a low abundant sub-phenotype next to mononuclear cells. Fluorescent labeling of these polynuclear cells allowed them to be purified from mononuclear cells by fluorescence-activated cell sorting (FACS) without inducing long-term toxicity. A later study by the same group demonstrated the applicability of image-guided SNAP for selective labeling of individual neurons in complex dense-cultured neuronal networks, thereby offering a valuable tool for studying neuron morphology, such as dendritic spine density [64]. Additionally, both Madrid and Saklayen provided a proof-of-concept of performing spatial-selective photoporation with their developed photothermal substrates (**Section 3.2**) [49,50].

5.2 Nanoparticle targeting

While laser beam targeting offers ultimate control, even down to a single-cell level, in some applications it is sufficient to target a particular cell type. In that case, it may be interesting to functionalize photothermal NPs with a specific ligand, offering high-affinity binding to that cell type. Over the years, several groups exploited this concept by functionalizing AuNPs with receptor-targeted antibodies for selective and amplified intracellular delivery [9,20,29,45–47]. For these purposes, the epidermal growth factor receptor on cancer cells has been targeted with antibody-functionalized AuNPs [20,29,45,46]. Other examples include targeting specific receptors on T cells [9] and retinal ganglion cells [47]. If the cells of interest have such a unique receptor, provided that ligands are available and can be functionally coupled to the NPs, this strategy is less complex than SNAP in the sense that no image analysis is needed to identify the target cells.

Studies by Yao et al. stated cell-selective binding as they demonstrated high-affinity targeting of functionalized AuNPs to the cells of interest compared to their non-functionalized counterparts [20,45]. However, it is important to note that absolute cell selectivity could not be

540 claimed as aspecific binding of functionalized AuNPs, VNB formation and subsequent delivery
541 was not assessed for non-target cells. It was the group of Lapotko that demonstrated that this
542 receptor-binding strategy could be effectively used to selectively target a subset of cells in
543 heterogeneous samples [9]. To achieve this, the authors used small AuNPs that are not large
544 enough to form VNBs themselves. However, by functionalizing them with an antibody targeted
545 toward a surface receptor, they achieved receptor-mediated endocytic uptake so that many of
546 the small AuNPs were present as a cluster in newly formed endosomes (close to the plasma
547 membrane). The induced AuNP clusters were large enough for effective laser absorption,
548 thermal-induced VNB formation and plasma membrane disruption. With this approach, they
549 demonstrated selective gene transfection of CD3-postive human T cells, while in the presence
550 of non-target CD3-negative peripheral blood mononuclear cells. Interestingly, the same group
551 used this strategy to also induce selective endosomal release of Doxil liposomes in cancer cells
552 [46]. Antibody-functionalized AuNPs were co-incubated with antibody-functionalized Doxil
553 liposomes upon which endocytic uptake was stimulated in the target cancer cells, but not in
554 normal cells. Endosomes in cancer cells were shown to contain mixed clusters of Doxil
555 liposomes and AuNPs, while in normal cells this co-localized clustering was virtually absent.
556 As a result, upon pulsed laser irradiation, cancer cells experienced more endosomal release of
557 the encapsulated chemotherapeutic doxorubicin opposed to the normal cells. Later on, they
558 demonstrated that this principle provided promising results *in vivo* as well, resulting in
559 improved tumor killing compared to Doxil liposomes alone [29]. Complementary to this
560 endosomal escape strategy, Huang et al. functionalized AuNPs with both targeting peptides and
561 siRNA, demonstrating selective gene knockdown in receptor-positive cells whereas non-target
562 cells were left untouched [65]. VNB-mediated photoporation for endosomal destabilization will
563 be elaborated on in **Section 6.2**. Finally, the Meunier group has explored the use of antibody-
564 functionalized AuNPs for plasma membrane disruption through plasma-induced VNBs [66]. A
565 recent study from the same group further highlighted the *in vivo* potential of this antibody-
566 targeting approach [47]. Retinal ganglion cells, located in the back of the eye, were successfully
567 targeted through the use of AuNPs functionalized with antibodies toward the enriched cell-
568 surface voltage gate K^+ channel subunit $K_v1.1$. Upon intravitreal injection of the antibody-
569 functionalized AuNPs mixed with the compounds of interest, cells were photoporated using
570 100 fs 800 nm (off-resonant) laser pulses and selective delivery of macromolecules such as
571 siRNA was achieved.

572 **6 Intracellular delivery: focus on effector molecules and target cells**

573 VNB-mediated photoporation has proven to be successful for intracellular delivery of a
574 variety of effector molecules in a broad range of cell types. The following sections will discuss
575 most recent advances in terms of effector molecules, target cells and applications in the field of
576 intracellular delivery. We will make a distinction depending on whether VNB-mediated
577 photoporation was used to permeabilize the plasma, endosomal or nuclear membrane.

578 *6.1 Plasma membrane disruption*

579 VNB-mediated photoporation at the level of the plasma membrane, followed by entry of
580 foreign compounds from the extracellular compartment into the cytosol (**Figure 5A**), has
581 demonstrated to be a suitable intracellular delivery method for a broad variety of adherent and
582 suspension cell types. Throughout the years, intracellular delivery of plasmid DNA (pDNA) by
583 VNB-mediated photoporation has probably been studied the most, even though reported results
584 are quite variable. Indeed, pDNA delivery has proven to be quite challenging, which is related
585 to its large size and negatively charged nature. Lukianova-Hleb et al. described successful
586 targeting and pDNA transfection of CD3-positive hard-to-transfect human T cells using
587 thermal-induced VNBs and antibody-functionalized AuNPs [9]. They reported that ~96% of
588 the target cells demonstrated green fluorescent protein (GFP) expression 48 h post laser
589 irradiation, while protein expression was only observed in ~10% of the non-target cells. This
590 was accompanied by a cell viability of ~75%, as determined via Calcein AM staining of live
591 cells combined with counting of trypan blue negative cells. Several reports by the group of
592 Meunier and Heisterkamp used plasma-induced VNBs from spherical AuNPs for pDNA
593 delivery but with variable success. Where Baumgart et al. (45 fs, λ=800 nm) reported ~23%
594 transfected human cancer melanoma cells [28], Schomaker et al. (120 fs, λ=796 nm) observed
595 negligible transfection of canine pleomorphic adenoma cells and below 5% transfected canine
596 CD34+ hematopoietic stem cells [12]. The former study reported a cell viability over 80%, as
597 determined by the MTT assay, whereas the latter measured Annexin V- and PI-stained dead
598 cells by flow cytometry and reported >80% and <40% cell viability for these cell lines,
599 respectively. In a recent study, Santra et al. generated thermal-induced VNBs from nano-
600 corrugated mushroom-shaped gold-coated polystyrene NPs and demonstrated successful
601 plasmid transfection in human cancer cells (~86%) and mouse embryonic stem cells (~73%)
602 [21]. This was accompanied by a high cell viability (~96%), as concluded from microscopy
603 analysis of live cells stained with Calcein AM. pDNA delivery through thermal-induced VNBs
604 and subsequent protein expression has also been proven successful for carbon black NPs
605 (**Section 3.1**). Chakravarty et al. reported that ~22% of laser-irradiated human prostate cancer

606 cells had taken up the pDNA and that luciferase expression was a 17-fold higher compared to
607 non-irradiated cells [34]. Cell viability, as measured with flow cytometry using PI staining of
608 dead cells, was for the optimal conditions >90%. The photothermal substrate reported by Man
609 et al. (**Section 3.2**) was able to deliver GFP-encoding plasmids into Ramos B cells reaching
610 ~58% GFP-positive cells 48 hours postdelivery [53]. Finally, apart from mammalian cells,
611 McGraw et al. recently proved the usefulness of VNB-mediated photoporation for pDNA
612 delivery in *S. cerevisiae*, as a model for fungal cells [43]. The authors hypothesized the
613 generation of plasma-induced VNBs, under pulsed laser irradiation, and reported a delivery
614 efficiency of ~30% accompanied by a cell viability close to 100%, as measured with flow
615 cytometry using 7-aminoactinomycin D (AAD) staining of dead cells. Of note, variabilities in
616 reported transfection results cannot solely be explained by the fact that some cell types are more
617 recalcitrant to transfection than others. Inconsistencies can be related to the use of different
618 assays for quantification of transfection efficiency, combined with in some cases a more
619 objective analysis of results. As a matter of fact, most of the reported values, especially the
620 highest ones, are based on fluorescence microscopy where the threshold for positive cells (i.e.,
621 cells to which pDNA was delivered and a fluorescent protein is produced) is not consistent
622 between studies, combined with the fact that it is not always clear if autofluorescence of control
623 cells is properly accounted for. In addition, the number of cells that are considered in typical
624 microscopy analysis is much less than what is the case for analysis by flow cytometry.
625 Strikingly, only three used analysis by flow cytometry, which also reported the lowest pDNA
626 transfection efficiencies [12,34,43]. As discussed in **Section 4**, inconsistencies in cell viabilities
627 can be attributed to the range of different assays and techniques available to determine this, one
628 more suitable than the other. Efficiency and viability results as reported for certain NPs and
629 laser parameters are summarized in **Table 1**.

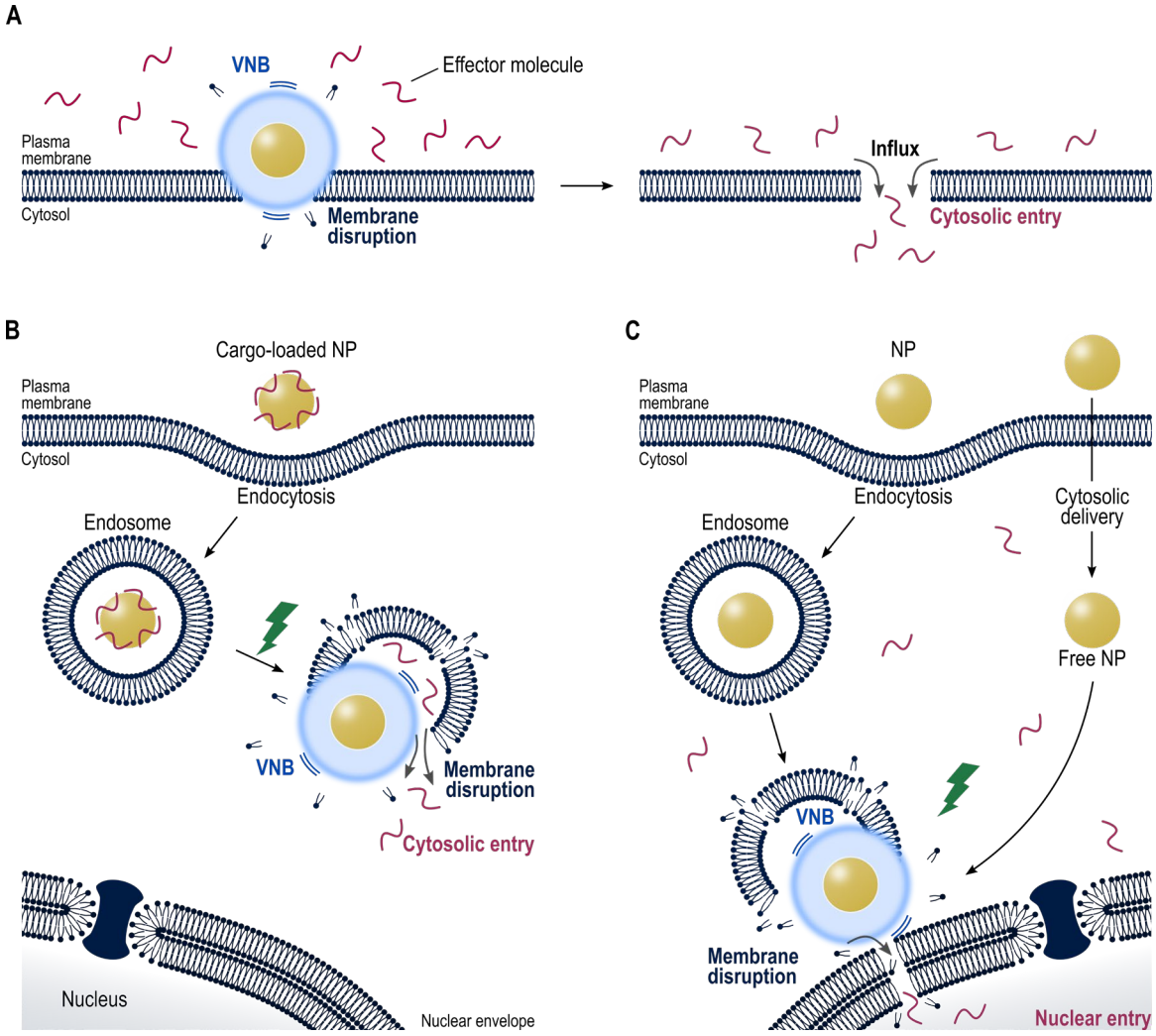

Figure 5. Schematic overview of VNB-induced membrane disruption at the level of the **A.** plasma membrane **B.** endosomal membrane and **C.** nuclear membrane. NP, nanoparticle; VNB, vapor nanobubble.

Apart from plasmids also RNA-based macromolecules are of interest, such as siRNA and messenger RNA (mRNA). Xiong et al., demonstrated in a comparative study that VNB-mediated plasma membrane disruption outperformed photothermal membrane heating for delivery of siRNA and subsequent gene knockdown in H1299 lung carcinoma cells [7]. Where a gene knockdown >80% was reported for thermal-induced VNBs, this was only ~40% in case of mere heating of membrane-associated AuNPs. Both laser regimes resulted in a cell viability >90%, as concluded from flow cytometry and microscopy analysis of live cells stained with Calcein AM. In a later study, Schomaker et al. applied plasma-induced VNBs for siRNA delivery in canine prostate cancer cells with the aim of downregulating the tumor driving oncogene HMGA2 and reported a significant drop of gene expression (<50%) compared to untreated cells [60]. This was accompanied by a cell viability >90%, as determined by flow

645 cytometry analysis of Annexin V- and PI-stained dead cells. Wayteck et al. studied thermal-
646 induced VNBs for siRNA delivery and gene knockdown in primary murine CD8+ cytotoxic T
647 cells aimed at boosting their anti-tumor response by downregulating immunosuppressive
648 pathways [62]. The authors reported 40-60% silencing of the CD45 gene, as a model target,
649 with a cell viability of ~70% as measured by the CellTiter-Glo® assay. VNB-mediated
650 photoporation for mRNA transfections was only recently reported for the first time by Raes et
651 al. in both adherent and suspension cells [14]. Owing to the rather instable nature of mRNA,
652 this study clearly emphasized the importance of washing steps before adding mRNA to cells in
653 order to remove degradative enzymes from the culture medium. Photoporation of HeLa cervical
654 cancer cells and hard-to-transfect Jurkat T cells, as a model for primary human T cells, resulted
655 respectively in ~38% and ~20% transfected cells for one photoporation run. This was
656 accompanied by a cell viability of ~80% and ~75%, respectively, as measured by the CellTiter-
657 Glo® assay. Considering that still many T cells were viable but untransfected, the authors treated
658 the cells two more times with VNB-mediated photoporation, improving the transfection
659 efficiency further to ~45%. Importantly, in the latter two studies the more gentle nature of VNB-
660 mediated photoporation for T cell transfections was demonstrated compared to electroporation,
661 which is the current standard physical transfection technique for hard-to-transfect immune cells.
662 Owing to VNB-mediated photoporation being more gentle to cells as compared to
663 electroporation, Wayteck and Raes reported threefold and fivefold higher numbers of
664 transfected and viable T cells, respectively [14,62].

665 Apart from nucleic acids, Thermal-induced VNBs have been used for the delivery of
666 bioactive proteins as well. For instance, Bošnjak et al. demonstrated intracellular delivery of
667 guide-RNA/Cas9 ribonucleoprotein complexes for genome editing in hard-to-transfect murine
668 CD8+ T cells (~5%) and lymph node stroma cells (~5%) [67]. Cytotoxic effect of photoporation
669 on these cell types were, however, not reported. Another example is given by the Chiou group
670 that delivered the bacterial enzyme β-lactamase into adherent human dermal fibroblasts and
671 Ramos B cells, respectively, using the BLAST platform [48] and the sharp-tipped microwell
672 arrays for capturing suspension cells [53] (**Section 3.2**). In particular they proved that laser
673 manipulation did not hinder biological activity of the enzyme. Van Hoecke et al. reported
674 hallmarks of necroptotic-like cell death (i.e., cell swelling and cell membrane rupture) upon
675 successful delivery of the mixed-lineage kinase domain-like (MLKL) protein in B16F10 mouse
676 melanoma cells [41]. This protein is considered one of the key terminal mediators of
677 necroptosis, which is a cell death mechanism with immunogenic properties. Combined with the

678 observed significant drop in cell viability (~62%), measured by the CellTiter-Glo® assay, it
679 shows that this strategy is of interest for anti-cancer immunotherapy. Finally, Yao et al. used
680 functionalized gold nanorods targeted toward the epidermal growth factor receptor on human
681 ovarian carcinoma cells and reached selective delivery of the anti-Ki-67 antibody in ~50% of
682 the target cells [20]. This was accompanied by a cell viability >80%, determined through
683 detection of PI-stained dead cells by flow cytometry.

684 Fluorescent labeling of cells for live-cell microscopy or *in vivo* tracking also benefits from
685 VNB-mediated photoporation as intracellular delivery strategy. By directly delivering contrast
686 molecules, like quantum dots or fluorescent polymers, in the cellular cytosol, Xiong et al.
687 reported intense cell labeling and extended *in vivo* tracking of labeled cells for many cell
688 generations, whereas this was not the case for endocytic uptake of the same contrast agent [8].
689 Interestingly, it was shown that cytosolic delivery of contrast agents avoids asymmetric
690 inheritance of the labels over daughter cells, in contrast to endocytic uptake, thereby improving
691 labeling uniformity of the cell population over extended periods of time. In a later study from
692 our group, Liu et al. used VNB-mediated photoporation to deliver membrane-impermeable
693 fluorescent contrast agents, like phalloidin, nanobodies and SNAP-tags in cells, thus facilitating
694 live-cell fluorescence microscopy investigations [31]. Interestingly, by using GQDs as
695 photothermal agents, the amount of delivered label could be carefully controlled by repeated
696 laser activation and VNB formation (**Section 3.1**). In a follow-up study, the authors focused on
697 the intracellular delivery of labeled nanobodies and demonstrated their suitability for long-term
698 live-cell fluorescence microscopy of specific subcellular structures [68]. These studies are
699 encouraging for VNB-mediated photoporation to become an enabling technology for efficient
700 labeling of cells for both *in vitro* microscopy studies as *in vivo* cell tracking applications.

701 *6.2 Endosomal membrane disruption*

702 Apart from permeabilizing the plasma membrane, laser-induced VNBs have also been
703 used to destabilize endosomal membranes in the context of nanocarrier-mediated delivery of
704 membrane-impermeable cargo. Nanocarriers are typically internalized by endocytic processes
705 so that they reside in endosomal vesicles after uptake. Efficient endosomal escape of the
706 nanocarriers and their cargo into the cytosol is, however, one of the most important bottlenecks
707 for efficient intracellular drug delivery. This is why photothermal nanoparticles have been
708 explored as potential destabilizers of endosomal membranes upon laser-induced VNB
709 formation. As illustrated in **Figure 5B**, once incubated with the cells, NPs are already quickly

710 transferred to the endosomal compartment. To establish endosomal membrane disruption and
711 cytosolic compound delivery in a controlled and on-demand manner, NPs are often loaded with
712 cargo molecules through electrostatic or covalent interactions. When VNBs are generated upon
713 pulsed laser irradiation, cavitation forces release the compounds from the NPs and induce their
714 endosomal leakage [42,61].

715 Early on, studies by the group of Reich described successful gene knockdown through
716 delivery of siRNA [65,69]. For instance, a study by Braun et al. reported ~80% of GFP silencing
717 in C116 cells when irradiating 40 nm hollow gold nanoshells coupled to siRNA (130 fs, λ=800
718 nm) [69]. Quantitative cell viability data was, however, not provided. In a recent study from the
719 same group, Morales et al. coupled a proapoptotic peptide (H_6PAD) as functional peptide and
720 a cell-penetrating peptide (TAT) as endocytic uptake enhancer to the surface of 40 nm hollow
721 gold nanoshells via a thiol-gold bond [70]. The authors demonstrated that, upon pulsed laser
722 irradiation of PPC-1 primary human prostate carcinoma cells, the peptides were released from
723 the NP's surface and successful endosomal leakage of the functional cargo was obtained. More
724 importantly, it seemed that the apoptotic response, incited by effector molecules released in the
725 cytosol, further amplified cell toxicity relative to laser treatment with non-functionalized NPs.
726 Another study used an identical approach to deliver Cre recombinase, which is a genome editing
727 enzyme [71]. Functional delivery and subsequent gene activation was observed in ~17% of the
728 laser-irradiated HeLa cervical cancer cells via this strategy, accompanied by a cell viability of
729 ~70% mainly attributed to the Cre recombinase toxicity (viability assay not reported). It should
730 be noted, however, that although laser conditions reported in the aforementioned studies
731 strongly suggest thermal-induced VNB formation as the underlying mechanism for endosomal
732 disruption, experimental proof for this was not provided. Instead, Vermeulen et al. recently
733 compared endosomal escape of JetPEI/pDNA/AuNP complexes (10 nm AuNPs) for low- and
734 high-intensity laser pulses (7 ns, λ=561 nm) that respectively generate endosomal escape based
735 on heat transfer and thermal-induced VNB generation [61]. Effective VNB formation was
736 confirmed with dark-field microscopy and led to more efficient endosomal membrane
737 disruption compared to the heat-mediated mechanism. Nevertheless, both photothermal effects
738 were unable to promote significant transfection as either pDNA was inevitably damaged by
739 VNB formation or heat-mediated pores were insufficiently large to facilitate effective
740 endosomal escape. From the same group, Fraire et al. used 95 nm positively charged
741 poly(diallyl dimethyl ammonium chloride)-functionalized AuNPs as carriers for siRNA and
742 studied their endosomal escape potential again in terms of the applied laser dose [42]. With the

743 use of two different cancer cell lines (H1299 and HeLa cells), the authors observed that for the
744 heating regime (i.e., low laser intensity) endosomal escape efficiency strongly depended on cell
745 type-related variabilities in endocytic internalization and clustering of the nanocomplexes.
746 Instead, for the VNB mode (i.e., high laser intensity) this was not the case, resulting in ~50%
747 gene knockdown in both cell types accompanied by a cell viability >70%, as measured by the
748 MTT assay. Interestingly, by pre-complexing siRNA onto the photothermal NPs, a 500-fold
749 lower siRNA concentration could be used than what is needed for plasma membrane
750 photoporation.

751 In conclusion, endosomal membrane photoporation enhanced by VNB formation offers
752 an alternative approach for classical plasma membrane photoporation. Especially the feature to
753 load cargo molecules onto photothermal NPs can drastically reduce the necessary doses of
754 expensive effector molecules like mRNA, nanobodies, and so on. Pitfalls, however, are related
755 with the irreversible destruction of large and sensitive compounds like pDNA, as demonstrated
756 in the study of Vermeulen et al. [61]. Further work is needed to optimize the design of such
757 photothermal nanocarriers thereby offering better protection to the cargo molecules while still
758 being able to destabilize the endosomal membrane.

759 *6.3 Nuclear envelope disruption*

760 The nuclear envelope is recognized as one of the most difficult cellular membranes to get
761 across, especially for large effector molecules (>40 kDa), such as pDNA, which cannot
762 spontaneously migrate through the nucleopore complexes. Recently it was explored if VNB-
763 mediated photoporation could induce transient nuclear envelope ruptures in a controlled manner
764 and thereby possibly lift this barrier for larger molecules [72,73]. **Figure 5C** schematically
765 illustrates this principle where nuclear envelope disruption and subsequent delivery can be
766 obtained by photothermal NPs either endocytosed or freely present in the cytosol. Li et al. used
767 plasmonic liposomes as optical perforation enhancers for pDNA delivery in hard-to-transfect
768 murine macrophages (RAW 264.7 cell line) [72]. pDNA was first delivered in the cytosol using
769 electroporation after which plasmonic liposomes were endocytosed and irradiated with 28 ps
770 750 nm pulsed laser light. The AuNPs decorating the liposomes generated thermal-induced
771 VNBs close to the nucleus, thereby disrupting both the endosomal and nuclear membrane as
772 was evidenced by the enhanced nuclear plasmid accumulation and gene expression after
773 photoporation (2.7-fold increase compared to electroporation alone). Cell viability was
774 qualitatively assessed by live/dead staining combined with microscopy imaging but not

quantified. A study published in the same year by Houthaeve et al. used 70 nm cationic AuNPs for VNB-mediated photoporation, which were either sequestered in the endosomes or cytosolically delivered via electroporation [73]. In both cases enrichment of AuNPs in the perinuclear region was observed over time. The authors used a modified HeLa cervical cancer cell line, stably transected with a GFP-coupled nuclear localization signal (NLS), that allowed for easy evaluation of VNB-induced nuclear envelope ruptures. As long as the nuclear envelope is intact, the GFP-NLS resides within the nucleus. Upon pulsed laser irradiation (7 ns, λ=561 nm), thermal-induced VNBs permeabilized the nuclear envelope, as evidenced from a sudden outflux of GFP-NLS into the cytosol. Within an hour, it was observed that GFP-NLS was recruited back into the nucleus, thereby confirming restoration of the nuclear envelope's integrity. The authors also demonstrated that the kinetics of these events were similar to those observed in spontaneous nuclear envelope ruptures in laminopathy patient cells. As such VNB-mediated photoporation of the nuclear envelope can be a valuable tool for fundamental biological research in the field of nuclear envelope disruption. Furthermore, in the same study intranuclear delivery of cytosolic effector molecules was shown as well. Using plasma membrane photoporation, the authors first delivered 70 kDa and 150 kDa FITC-dextran molecules to the cytosol of HeLa cervical cancer cells. Being too large to spontaneously pass through the nucleopore complexes, they remain exclusively in the cellular cytosol. However, upon VNB-induced permeabilization of the nuclear envelope using AuNPs as described above, both molecule sizes were observed to quickly flow inside the nuclear compartment. Although this study showed that laser-induced VNB formation can be used for the controlled disruption of the nuclear envelope, the percentage of cells in which this could be successfully performed was very low (<5%). This is due to the fact that endocytosis or electroporation of photothermal NPs does not guarantee exclusive targeting of them toward the perinuclear area. Part of the NPs may still be at more peripheral sites in the cell, causing collateral damage upon laser irradiation. And even when they are in the perinuclear area, their distance to the nuclear envelope may still be too large for effective pore formation. Therefore, to make this approach useable in the future it will be important to find ways to selectively target photothermal NPs to the nuclear envelope.

7 Conclusions and perspectives

VNB-mediated photoporation has, over the years, developed into a versatile intracellular delivery tool. It has been shown to be able to compromise the integrity of the plasma membrane next to destabilizing endosomes and even the nuclear envelope. Furthermore, this technique has demonstrated to be very versatile in terms of cell types and membrane-impermeable effector

808 molecules that can be delivered, although further work is still needed to enhance delivery of
809 very large molecules such as pDNA and mRNA. When properly optimized, VNB-mediated
810 photoporation proved to be quite gentle to the cells thanks to limiting the inflicted damage to
811 the immediate vicinity of the photothermal NPs. Still, more research is needed to investigate
812 cellular responses following membrane disruption, which may provide further insights on how
813 to limit cell stress even more. Importantly, in this context, it would be valuable that future
814 studies systematically demonstrate actual VNB formation rather than just assume this
815 phenomenon based on the applied laser conditions. We anticipate that this would provide a
816 more consistent and complete picture of the impact of laser-induced VNBs on cells.

817 Although the protocol for photoporation with photothermal NPs is very straightforward, it
818 remains an open question if NPs in contact with cells may induce unwanted effects on the long
819 term [74]. Especially if one would think of using this technology for producing engineered
820 therapeutic cells, NP-induced cytotoxicity can be of concern. In that sense, the various
821 photothermal substrates that have emerged in recent years are quite interesting since they offer
822 similar possibilities while avoiding exposure of cells to NPs. They do require, however,
823 advanced production techniques that can hinder widespread use while upscaling for sufficient
824 throughput remains to be demonstrated.

825 Up until now, applications of photoporation for *in vivo* intracellular delivery are rather
826 scarce. Undoubtedly this is due to the limited tissue penetration of light, which limits broad
827 applicability, although NIR-responsive photothermal NPs offer opportunities in this regard.
828 Depending on the target, it will be needed to direct the photothermal NPs specifically to the cell
829 types of interest, apart from the effector molecules that should reach the same target site as well.
830 Targeting of NPs and drug molecules is being heavily studied in the field of nanomedicine-
831 mediated drug delivery and findings from that area may proof to be useful for translating
832 photoporation to *in vivo* applications as well. Application areas that seem particularly feasible
833 are the skin and dedicated parts in the eye. Especially since clinical laser technology is already
834 used for treatment of certain kinds of skin and ophthalmic pathologies.

835 Finally, it is quite interesting to see that very recently other (*in vivo*) applications of laser-
836 induced VNB generation are emerging beyond intracellular delivery. It was shown that laser-
837 induced VNBs from photothermal NPs can gently but decisively alter the microstructure of
838 bacterial biofilms, substantially enhancing drug diffusion and improving the efficacy of
839 antibiotics up to several orders of magnitude [33,75]. In another recent study, laser-induced

VNBs were demonstrated to be able to destroy vision-impairing vitreous opacities in human eyes at substantially reduced light energies as compared to current laser therapies [76]. At last, VNB-mediated detection and destruction of melanoma circulating tumor cells was explored as well, harnessing their elevated melanin content as photothermal sensitizer [77]. Together it shows that the potential of laser-induced VNBs, even though discovered already 20 years ago, continues to grow for a diversity of biomedical applications where precise mechanical alteration of a biological barrier is needed.

Declaration of competing interest

The authors declare that they have no known competing financial interests or personal relationships that could have appeared to influence the work reported in this paper.

Acknowledgements

This work was supported by funding of the Research Foundation Flanders (FWO, grant numbers 1110719N, 1500418N and 12Q8718N). The funding by the European Research Council (ERC) under the European Union's Horizon 2020 research and innovation program (grant number 648124) is acknowledged with gratitude.

857 **Table 1.** Summary of different NPs with respect to material, morphology, size and surface functionalization explored for cytosolic delivery via
858 VNB-mediated plasma membrane disruption.

Material and morphology	Size	Surface Functionalization	Effector molecule	Clustering?	Pulse duration, wavelength	Cell type	Efficiency	Viability	Ref
Gold	30 nm	Anti-EGFR Ab	FD 150 kDa	Not specified	4 ns, 532 nm	OVCAR-3	~70%	>80% (*)	[45]
Nanospheres	60 nm	OKT 3 Ab	pDNA	Yes	70 ps, 532 nm	CD3+ T	~96%	~75%	[9]
		PDDAC	MLKL protein	No	7 ns, 561 nm	B16F10	~38%	-	[41]
		PDDAC	mRNA	No	7 ns, 561 nm	HeLa	~38%	~80%	[14]
						Jurkat	~20%	~75%	[14]
	70 nm	Amine polymerization	siRNA	No	7 ns, 561 nm	H1299	>80%	>90%	[7]
						CD8+ T	40-60%	~70%	[62]
	100 nm	-	pDNA	Yes	45 fs, 800 nm	WM278	~23%	>80%	[28]
	200 nm	-	pDNA	Not specified	120 fs, 796 nm	ZMTH3	~0.57%	>80% (*)	[12]
						CD34+ HS	~2.7%	<40% (*)	[12]
		-	Guide-RNA/Cas9	Not specified	850 ps, 532 nm	CD8+ T	~5%	-	[67]
						Stroma	~5%	-	[67]
	250 nm	-	siRNA	Yes	120 fs, 796 nm	CT1258	<50%	>90% (*)	[60]

Gold nanorods	Not specified	Anti-EGFR Ab	Anti-Ki-46	Not specified	4 ns, 532 nm	OVCAR-3	~54%	>80% (*)	[20]
					4 ns, 730 nm	OVCAR-3	~49%	>80% (*)	[20]
Gold core-shell NPs	300 nm	PEG	pDNA	No	5 ns, 945 nm	CL1-0	~86%	~96%	[21]
						P19	~73%	~96%	[21]
Carbon Black NPs	25 nm	SDS	pDNA	Yes (200 nm)	100 fs, 800 nm	DU 145	~22%	>90% (*)	[34]
GQDs	40 nm	-	FD 10 kDa	Yes	7 ns, 561 nm	HeLa	>50%	>80%	[31]
	28 nm	PEG	FD 10 kDa	No	7 ns, 561 nm	Jurkat	~56%	~80%	[13]
rGO	241 nm	PEG	FD 10 kDa	No	7 ns, 561 nm	Jurkat	~63%	~80%	[13]
	266 nm	PEI	FD 10 kDa	No	2 ps, 800 nm	Jurkat	~80%	~80%	[13]

859 Ab, antibody; EGFR, epidermal growth factor receptor; FD, FITC-Dextran; GQDs, graphene quantum dots; HS, hematopoietic stem; MLKL,
860 mixed-lineage kinase domain-like; mRNA, messenger RNA; NPs, nanoparticles; PDDAC poly(diallyl dimethyl ammonium chloride); pDNA,
861 plasmid DNA; PEG, polyethylene glycol; PEI, polyethylenimine; rGO, reduced graphene oxide; SDS Sodium dodecyl sulphate; siRNA, small
862 interfering RNA.

863 (*) Cell viability assessment via live/dead staining and analysis by flow cytometry

864

865 Papers of particular interest, published within the period of review, have been highlighted as:

866 * of special interest

867 ** of outstanding interest

868 [1] M.P. Stewart, R. Langer, K.F. Jensen, Intracellular delivery by membrane disruption:
869 Mechanisms, strategies, and concepts, Chem. Rev. 118 (2018) 7409–7531.
870 https://doi.org/10.1021/acs.chemrev.7b00678.

871 [2] M.P. Stewart, A. Sharei, X. Ding, G. Sahay, R. Langer, K.F. Jensen, In vitro and ex
872 vivo strategies for intracellular delivery, Nature. 538 (2016) 183–192.
873 https://doi.org/10.1038/nature19764.

874 [3] M.P. Stewart, A. Lorenz, J. Dahlman, G. Sahay, Challenges in carrier-mediated
875 intracellular delivery: Moving beyond endosomal barriers, WIREs Nanomed
876 Nanobiotechnol. 8 (2016) 465–478. https://doi.org/10.1002/wnan.1377.

877 [4] X. Du, J. Wang, Q. Zhou, L. Zhang, S. Wang, Z. Zhang, C. Yao, Advanced physical
878 techniques for gene delivery based on membrane perforation, Drug Deliv. 25 (2018)
879 1516–1525. https://doi.org/10.1080/10717544.2018.1480674.

880 [5] R. Xiong, S.K. Samal, J. Demeester, A.G. Skirtach, S.C. De Smedt, K. Braeckmans,
881 Laser-assisted photoporation: fundamentals, technological advances and applications,
882 Adv. Phys. X. 1 (2016) 596–620. https://doi.org/10.1080/23746149.2016.1228476.

883 [6] E. Lukianova-Hleb, Y. Hu, L. Latterini, L. Tarpani, S. Lee, R.A. Drezek, J.H. Hafner,
884 D.O. Lapotko, Plasmonic Nanobubbles as Transient Vapor Nanobubbles Generated
885 around Plasmonic Nanoparticles, ACS Nano. 4 (2010) 2109–2123.
886 https://doi.org/10.1021/nn1000222.

887 [7] R. Xiong, K. Raemdonck, K. Peynshaert, I. Lentacker, I. De Cock, J. Demeester, S.C.
888 De Smedt, A.G. Skirtach, K. Braeckmans, Comparison of Gold Nanoparticle Mediated
889 Photoporation: Vapor Nanobubbles Outperform Direct Heating for Delivering
890 Macromolecules in Live Cells, ACS Nano. 8 (2014) 6288–6296.
891 https://doi.org/10.1021/nn5017742.

892 [8] R. Xiong, F. Joris, S. Liang, R. De Rycke, S. Lippens, J. Demeester, A. Skirtach, K.
893 Raemdonck, U. Himmelreich, S.C. De Smedt, K. Braeckmans, Cytosolic Delivery of

894 Nanolabels Prevents Their Asymmetric Inheritance and Enables Extended Quantitative
895 in Vivo Cell Imaging, Nano Lett. 16 (2016) 5975–5986.
896 https://doi.org/10.1021/acs.nanolett.6b01411.

897 [9] E.Y. Lukianova-Hleb, D.S. Wagner, M.K. Brenner, D.O. Lapotko, Cell-specific
898 transmembrane injection of molecular cargo with gold nanoparticle-generated transient
899 plasmonic nanobubbles, Biomaterials. 33 (2012) 5441–5450.
900 https://doi.org/10.1016/j.biomaterials.2012.03.077.

901 [10] É. Boulais, R. Lachaine, M. Meunier, Plasma Mediated off-Resonance Plasmonic
902 Enhanced Ultrafast Laser-Induced Nanocavitation, Nano Lett. 12 (2012) 4763–4769.
903 https://doi.org/10.1021/nl302200w.

904 [11] R. Lachaine, É. Boulais, M. Meunier, From Thermo- to Plasma-Mediated Ultrafast
905 Laser-Induced Plasmonic Nanobubbles, ACS Photonics. 1 (2014) 331–336.
906 https://doi.org/10.1021/ph400018s.

907 [12] M. Schomaker, D. Killian, S. Willenbrock, D. Heinemann, S. Kalies, A. Ngezahayo, I.
908 Nolte, T. Ripken, C. Junghanß, H. Meyer, H.M. Escobar, A. Heisterkamp, Biophysical
909 effects in off-resonant gold nanoparticle mediated (GNOME) laser transfection of cell
910 lines, primary- and stem cells using fs laser pulses, J. Biophotonics. 8 (2015) 646–658.
911 https://doi.org/10.1002/jbio.201400065.

912 [13] J. Liu, C. Li, T. Brans, A. Harizaj, S. Van de Steene, T. De Beer, S. De Smedt, S.
913 Szunerits, R. Boukherroub, R. Xiong, K. Braeckmans, Surface functionalization with
914 polyethylene glycol and polyethyleneimine improves the performance of graphene-
915 based materials for safe and efficient intracellular delivery by laser-induced
916 photoporation, Int. J. Mol. Sci. 21 (2020) 1540. https://doi.org/10.3390/ijms21041540.

917 [14] L. Raes, S. Stremersch, J.C. Fraire, T. Brans, G. Goetgeluk, S. De Munter, L. Van
918 Hoecke, R. Verbeke, J. Van Hoeck, R. Xiong, X. Saelens, B. Vandekerckhove, S. De
919 Smedt, K. Raemdonck, K. Braeckmans, Intracellular Delivery of mRNA in Adherent
920 and Suspension Cells by Vapor Nanobubble Photoporation, Nano-Micro Lett. 12
921 (2020) 185. https://doi.org/10.1007/s40820-020-00523-0.

922 **** This work reports for the first time the use of vapor nanobubble-mediated**
923 **photoporation for mRNA delivery and emphasizes the importance of transfection**

buffers and washing steps to preclude mRNA degradation.

[15] R. Xiong, C. Drullion, P. Verstraelen, J. Demeester, A.G. Skirtach, C. Abbadie, W.H. De Vos, S.C. De Smedt, K. Braeckmans, Fast spatial-selective delivery into live cells, J. Control. Release. 266 (2017) 198–204. https://doi.org/10.1016/j.jconrel.2017.09.033.

[16] K.A. Willets, R.P. Van Duyne, Localized Surface Plasmon Resonance Spectroscopy and Sensing, Annu. Rev. Phys. Chem. 58 (2007) 267–297. https://doi.org/10.1146/annurev.physchem.58.032806.104607.

[17] E. Boulais, R. Lachaine, A. Hatef, M. Meunier, Plasmonics for pulsed-laser cell nanosurgery: Fundamentals and applications, J. Photochem. Photobiol. C. 17 (2013) 26–49. https://doi.org/10.1016/j.jphotochemrev.2013.06.001.

[18] S. Hashimoto, D. Werner, T. Uwada, Studies on the interaction of pulsed lasers with plasmonic gold nanoparticles toward light manipulation, heat management, and nanofabrication, J. Photochem. Photobiol. C. 13 (2012) 28–54. https://doi.org/10.1016/j.jphotochemrev.2012.01.001.

[19] É. Boulais, R. Lachaine, M. Meunier, Plasma-Mediated Nanocavitation and Photothermal Effects in Ultrafast Laser Irradiation of Gold Nanorods in Water, J. Phys. Chem. C. 117 (2013) 9386–9396. https://doi.org/10.1021/jp312475h.

[20] C. Yao, F. Rudnitzki, Y. He, Z. Zhang, G. Hüttmann, R. Rahmanzadeh, Cancer cell-specific protein delivery by optoporation with laser-irradiated gold nanorods, J. Biophotonics. 13 (2020) e202000017. https://doi.org/10.1002/jbio.202000017.

[21] T.S. Santra, S. Kar, T.-C. Chen, C.-W. Chen, J. Borana, M.-C. Lee, F.-G. Tseng, Near-infrared nanosecond-pulsed laser-activated highly efficient intracellular delivery mediated by nano-corrugated mushroom-shaped gold-coated polystyrene nanoparticles, Nanoscale. 12 (2020) 12057–12067. https://doi.org/10.1039/d0nr01792b.

*** The synthetized core-shell nanoparticles induce strong hotspot formation around the nano-corrugated edges enclosing the nanoparticle's surface. Based on theoretical considerations, this should allow for vapor nanobubbles to be generated at a lower laser fluence relative to non-corrugated spherical core-shell nanoparticles.**

[22] T. Pylaev, E. Vanzha, E. Avdeeva, B. Khlebtsov, N. Khlebtsov, A novel cell

transfection platform based on laser optoporation mediated by Au nanostar layers, J. Biophotonics. 12 (2019) e201800166. https://doi.org/10.1002/jbio.201800166.

[23] D. Lapotko, Optical excitation and detection of vapor bubbles around plasmonic nanoparticles, Opt. Express. 17 (2009) 2538–2556. https://doi.org/10.1364/oe.17.002538.

[24] A. Siems, S.A.L. Weber, J. Boneberg, A. Plech, Thermodynamics of nanosecond nanobubble formation at laser-excited metal nanoparticles, New J. Phys. 13 (2011) 043018. https://doi.org/10.1088/1367-2630/13/4/043018.

[25] D. Lapotko, Pulsed photothermal heating of the media during bubble generation around gold nanoparticles, Int. J. Heat Mass Transf. 52 (2009) 1540–1543. https://doi.org/10.1016/j.ijheatmasstransfer.2008.08.010.

[26] A. Hatef, S. Fortin-Deschênes, E. Boulais, F. Lesage, M. Meunier, Photothermal response of hollow gold nanoshell to laser irradiation: Continuous wave, short and ultrashort pulse, Int. J. Heat Mass Transf. 89 (2015) 866–871. https://doi.org/10.1016/j.ijheatmasstransfer.2015.05.071.

[27] E.Y. Lukianova-Hleb, A.N. Volkov, D.O. Lapotko, Laser Pulse Duration is Critical for the Generation of Plasmonic Nanobubbles, Langmuir. 30 (2014) 7425–7434. https://doi.org/10.1021/la5015362.

[28] J. Baumgart, L. Humbert, É. Boulais, R. Lachaine, J.J. Lebrun, M. Meunier, Off-resonance plasmonic enhanced femtosecond laser optoporation and transfection of cancer cells, Biomaterials. 33 (2012) 2345–2350. https://doi.org/10.1016/j.biomaterials.2011.11.062.

[29] E.Y. Lukianova-Hleb, X. Ren, R.R. Sawant, X. Wu, V.P. Torchilin, D.O. Lapotko, On-demand intracellular amplification of chemoradiation with cancer-specific plasmonic nanobubbles, Nat. Med. 20 (2014) 778–784. https://doi.org/10.1038/nm.3484.

[30] E.Y. Lukianova-Hleb, D.O. Lapotko, Photothermal properties of gold nanoparticles under exposure to high optical energies, Nanotechnology. 19 (2008) 355702. https://doi.org/10.1088/0957-4484/19/35/355702.

[31] J. Liu, R. Xiong, T. Brans, S. Lippens, E. Parthoens, F.C. Zanacchi, R. Magrassi, S.K.

982 Singh, S. Kurungot, S. Szunerits, H. Bové, M. Ameloot, J.C. Fraire, E. Teirlinck, S.K.
983 Samal, R. De Rycke, G. Houthaeve, S.C. De Smedt, R. Boukherroub, K. Braeckmans,
984 Repeated photoporation with graphene quantum dots enables homogeneous labeling of
985 live cells with extrinsic markers for fluorescence microscopy, Light Sci. Appl. 7 (2018)
986 47. https://doi.org/10.1038/s41377-018-0048-3.

987 **** This paper demonstrates the potential to generate multiple vapor nanobubbles from**
988 **graphene quantum dots (opposed to gold nanoparticles) upon pulsed laser irradiation,**
989 **hence providing careful control of contrast agent delivery in cells.**

990 [32] D.O. Lapotko, Plasmonic nanoparticle-generated photothermal bubbles and their
991 biomedical applications, Nanomedicine. 4 (2009) 813–845.
992 https://doi.org/10.2217/nnm.09.59.

993 [33] E. Teirlinck, R. Xiong, T. Brans, K. Forier, J. Fraire, H. Van Acker, N. Matthijs, R. De
994 Rycke, S.C. De Smedt, T. Coenye, K. Braeckmans, Laser-induced vapour nanobubbles
995 improve drug diffusion and efficiency in bacterial biofilms, Nat. Commun. 9 (2018)
996 4518. https://doi.org/10.1038/s41467-018-06884-w.

997 [34] P. Chakravarty, W. Qian, M.A. El-Sayed, M.R. Prausnitz, Delivery of molecules into
998 cells using carbon nanoparticles activated by femtosecond laser pulses, Nat.
999 Nanotechnol. 5 (2010) 607–611. https://doi.org/10.1038/nnano.2010.126.

1000 [35] A. Sengupta, S.C. Kelly, N. Dwivedi, N. Thadhani, M.R. Prausnitz, Efficient
1001 Intracellular Delivery of Molecules with High Cell Viability Using Nanosecond-Pulsed
1002 Laser-Activated Carbon Nanoparticles, ACS Nano. 8 (2014) 2889–2899.
1003 https://doi.org/10.1021/nn500100x.

1004 [36] A. Sengupta, M.D. Gray, S.C. Kelly, S.Y. Holguin, N.N. Thadhani, M.R. Prausnitz,
1005 Energy Transfer Mechanisms during Molecular Delivery to Cells by Laser-Activated
1006 Carbon Nanoparticles, Biophys. J. 112 (2017) 1258–1269.
1007 https://doi.org/10.1016/j.bpj.2017.02.007.

1008 [37] C. Jumelle, C. Mauclair, J. Houzet, A. Bernard, Z. He, F. Forest, M. Peoc'h, S.
1009 Acquart, P. Gain, G. Thuret, Delivery of Molecules into Human Corneal Endothelial
1010 Cells by Carbon Nanoparticles Activated by Femtosecond Laser, PLoS One. 10 (2015)
1011 e0132023. https://doi.org/10.1371/journal.pone.0132023.

1012 [38] C. Jumelle, C. Mauclair, J. Houzet, A. Bernard, Z. He, F. Forest, C. Perrache, P. Gain,
1013 G. Thuret, Delivery of macromolecules into the endothelium of whole ex vivo human
1014 cornea by femtosecond laser-activated carbon nanoparticles, Br. J. Ophthalmol. 100
1015 (2016) 1151–1156. https://doi.org/10.1136/bjophthalmol-2015-307610.

1016 [39] S.Y. Holguin, M.D. Gray, P. Joseph, N.N. Thadhani, M.R. Prausnitz, Photoporation
1017 Using Carbon Nanotubes for Intracellular Delivery of Molecules and Its Relationship
1018 to Photoacoustic Pressure, Adv. Healthc. Mater. 7 (2018) 1701007.
1019 https://doi.org/10.1002/adhm.201701007.

1020 [40] L. Raes, C. Van Hecke, J. Michiels, S. Stremersch, J.C. Fraire, T. Brans, R. Xiong, S.
1021 De Smedt, L. Vandekerckhove, K. Raemdonck, K. Braeckmans, Gold Nanoparticle-
1022 Mediated Photoporation Enables Delivery of Macromolecules over a Wide Range of
1023 Molecular Weights in Human CD4+ T Cells, Crystals. 9 (2019) 411.
1024 https://doi.org/10.3390/cryst9080411.

1025 [41] L. Van Hoecke, L. Raes, S. Stremersch, T. Brans, J.C. Fraire, R. Roelandt, W.
1026 Declercq, P. Vandenabeele, K. Raemdonck, K. Braeckmans, X. Saelens, Delivery of
1027 Mixed-Lineage Kinase Domain-Like Protein by Vapor Nanobubble Photoporation
1028 Induces Necroptotic-Like Cell Death in Tumor Cells, Int. J. Mol. Sci. 20 (2019) 4254.
1029 https://doi.org/10.3390/ijms20174254.

1030 [42] J.C. Fraire, G. Houthaeve, J. Liu, L. Raes, L. Vermeulen, S. Stremersch, T. Brans, G.
1031 García-Díaz Barriga, S. De Keulenaer, F. Van Nieuwerburgh, R. De Rycke, J.
1032 Vandesompele, P. Mestdagh, K. Raemdonck, W.H. De Vos, S. De Smedt, K.
1033 Braeckmans, Vapor nanobubble is the more reliable photothermal mechanism for
1034 inducing endosomal escape of siRNA without disturbing cell homeostasis, J. Control.
1035 Release. 319 (2020) 262–275. https://doi.org/10.1016/j.jconrel.2019.12.050.

1036 **** By mapping subtle vapor nanobubble-induced alterations of cell processes at the**
1037 **transcriptome level, this study provides more in-depth knowledge regarding cell**
1038 **functionality upon laser treatment. Additionally, it was demonstrated that endosomal**
1039 **disruption is more robustly obtained by vapor nanobubbles instead of heating, resulting**
1040 **in successful siRNA delivery and gene knockdown.**

1041 [43] E. McGraw, R.H. Dissanayaka, J.C. Vaughan, N. Kunte, G. Mills, G.M. Laurent, L.A.
1042 Avila, Laser-Assisted Delivery of Molecules in Fungal Cells, ACS Appl. Bio Mater. 3

1043 (2020) 6167–6176. https://doi.org/10.1021/acsabm.0c00720.

1044 [44] C. Yao, R. Rahmanzadeh, E. Endl, Z. Zhang, J. Gerdes, G. Hüttmann, Elevation of
1045 plasma membrane permeability by laser irradiation of selectively bound nanoparticles,
1046 J. Biomed. Opt. 10 (2005) 064012. https://doi.org/10.1117/1.2137321.

1047 [45] C. Yao, F. Rudnitzki, G. Hüttmann, Z. Zhang, R. Rahmanzadeh, Important factors for
1048 cell-membrane permeabilization by gold nanoparticles activated by nanosecond-laser
1049 irradiation, Int. J. Nanomedicine. 12 (2017) 5659–5672.
1050 https://doi.org/10.2147/IJN.S140620.

1051 [46] E.Y. Lukianova-Hleb, A. Belyanin, S. Kashinath, X. Wu, D.O. Lapotko, Plasmonic
1052 nanobubble-enhanced endosomal escape processes for selective and guided
1053 intracellular delivery of chemotherapy to drug-resistant cancer cells, Biomaterials. 33
1054 (2012) 1821–1826. https://doi.org/10.1016/j.biomaterials.2011.11.015.

1055 [47] A.M. Wilson, J. Mazzaferri, É. Bergeron, S. Patskovsky, P. Marcoux-Valiquette, S.
1056 Costantino, P. Sapieha, M. Meunier, In Vivo Laser-Mediated Retinal Ganglion Cell
1057 Optoporation Using KV1.1 Conjugated Gold Nanoparticles, Nano Lett. 18 (2018)
1058 6981–6988. https://doi.org/10.1021/acs.nanolett.8b02896.

1059 **** Antibody-functionalized gold nanoparticles were successfully targeted toward retinal
1060 ganglion cells which leveraged selective siRNA delivery in an in vivo context.**

1061 [48] Y.C. Wu, T.-H. Wu, D.L. Clemens, B.-Y. Lee, X. Wen, M.A. Horwitz, M.A. Teitell,
1062 P.-Y. Chiou, Massively parallel delivery of large cargo into mammalian cells with light
1063 pulses, Nat. Methods. 12 (2015) 439–444. https://doi.org/10.1038/nmeth.3357.

1064 [49] M. Madrid, N. Saklayen, W. Shen, M. Huber, N. Vogel, E. Mazur, Laser-Activated
1065 Self-Assembled Thermoplasmonic Nanocavity Substrates for Intracellular Delivery,
1066 ACS Appl. Bio Mater. 1 (2018) 1793–1799. https://doi.org/10.1021/acsabm.8b00447.

1067 [50] N. Saklayen, M. Huber, M. Madrid, V. Nuzzo, D.I. Vulis, W. Shen, J. Nelson, A.A.
1068 McClelland, A. Heisterkamp, E. Mazur, Intracellular Delivery Using Nanosecond-
1069 Laser Excitation of Large-Area Plasmonic Substrates, ACS Nano. 11 (2017) 3671–
1070 3680. https://doi.org/10.1021/acsnano.6b08162.

1071 [51] A. Raun, N. Saklayen, C. Zgrabik, W. Shen, M. Madrid, M. Huber, E. Hu, E. Mazur, A

1072 comparison of inverted and upright laser-activated titanium nitride micropyramids for
1073 intracellular delivery, Sci. Rep. 8 (2018) 15595. https://doi.org/10.1038/s41598-018-
1074 33885-y.

1075 [52] C. Zhao, T. Man, X. Xu, Q. Yang, W. Liu, S.J. Jonas, M.A. Teitell, P.-Y. Chiou, P.S.
1076 Weiss, Photothermal Intracellular Delivery Using Gold Nanodisk Arrays, ACS Mater.
1077 Lett. 2 (2020) 1475–1483. https://doi.org/10.1021/acsmaterialslett.0c00428.

1078 [53] T. Man, X. Zhu, Y.T. Chow, E.R. Dawson, X. Wen, A.N. Patananan, T.L. Liu, C.
1079 Zhao, C. Wu, J.S. Hong, P.S. Chung, D.L. Clemens, B.Y. Lee, P.S. Weiss, M.A.
1080 Teitell, P.Y. Chiou, Intracellular Photothermal Delivery for Suspension Cells Using
1081 Sharp Nanoscale Tips in Microwells, ACS Nano. 13 (2019) 10835–10844.
1082 https://doi.org/10.1021/acsnano.9b06025.

1083 *** The authors manufactured a photothermal substrate that is able to trap suspension**
1084 **cells and thereby efficiently deliver the enzyme β-lactamase through vapor nanobubble-**
1085 **mediated photoporation.**

1086 [54] P. Shinde, S. Kar, M. Loganathan, H.-Y. Chang, F.-G. Tseng, M. Nagai, T.S. Santra,
1087 Infrared Pulse Laser-Activated Highly Efficient Intracellular Delivery Using Titanium
1088 Microdish Device, ACS Biomater. Sci. Eng. 6 (2020) 5645–5652.
1089 https://doi.org/10.1021/acsbiomaterials.0c00785.

1090 *** This paper describes a titanium microsdish device that, when it is mounted on top of**
1091 **the cell layer, promotes intracellular delivery through vapor nanobubble formation**
1092 **without relying on adhesion of nanoparticles to cells for pore formation.**

1093 [55] S. Kalies, G.C. Antonopoulos, M.S. Rakoski, D. Heinemann, M. Schomaker, T.
1094 Ripken, H. Meyer, Investigation of biophysical mechanisms in gold nanoparticle
1095 mediated laser manipulation of cells using a multimodal holographic and fluorescence
1096 imaging setup, PLoS One. 10 (2015) 1–20.
1097 https://doi.org/10.1371/journal.pone.0124052.

1098 [56] A.M. Moe, A.E. Golding, W.M. Bement, Cell healing: Calcium, repair and
1099 regeneration, Semin. Cell Dev. Biol. 45 (2015) 18–23.
1100 https://doi.org/10.1016/j.semcdb.2015.09.026.

1101 [57] M. Bischofberger, I. Iacovache, F. Gisou Van Der Goot, Pathogenic Pore-Forming

1102 Proteins: Function and Host Response, Cell Host Microbe. 12 (2012) 266–275.
1103 https://doi.org/10.1016/j.chom.2012.08.005.

1104 [58] N. Saklayen, S. Kalies, M. Madrid, V. Nuzzo, M. Huber, W. Shen, J. Sinanan-Singh,
1105 D. Heinemann, A. Heisterkamp, E. Mazur, Analysis of poration-induced changes in
1106 cells from laser-activated plasmonic substrates, Biomed. Opt. Express. 8 (2017) 4756.
1107 https://doi.org/10.1364/boe.8.004756.

1108 [59] Y. Zhang, X. Chen, C. Gueydan, J. Han, Plasma membrane changes during
1109 programmed cell deaths, Cell Res. 28 (2018) 9–21.
1110 https://doi.org/10.1038/cr.2017.133.

1111 [60] M. Schomaker, D. Heinemann, S. Kalies, S. Willenbrock, S. Wagner, I. Nolte, T.
1112 Ripken, H.M. Escobar, H. Meyer, A. Heisterkamp, Characterization of nanoparticle
1113 mediated laser transfection by femtosecond laser pulses for applications in molecular
1114 medicine, J. Nanobiotechnology. 13 (2015) 10. https://doi.org/10.1186/s12951-014-
1115 0057-1.

1116 [61] L.M.P. Vermeulen, J.C. Fraire, L. Raes, E. De Meester, S. De Keulenaer, F. Van
1117 Nieuwerburgh, S. De Smedt, K. Remaut, K. Braeckmans, Photothermally Triggered
1118 Endosomal Escape and its Influence on Transfection Efficiency of Gold-Functionalized
1119 JetPEI/pDNA Nanoparticles, Int. J. Mol. Sci. 19 (2018) 2400.
1120 https://doi.org/10.3390/ijms19082400.

1121 [62] L. Wayteck, R. Xiong, K. Braeckmans, S.C. De Smedt, K. Raemdonck, Comparing
1122 photoporation and nucleofection for delivery of small interfering RNA to cytotoxic T
1123 cells, J. Control. Release. 267 (2017) 154–162.
1124 https://doi.org/10.1016/j.jconrel.2017.08.002.

1125 [63] T. DiTommaso, J.M. Cole, L. Cassereau, J.A. Buggé, J.L. Sikora Hanson, D.T.
1126 Bridgen, B.D. Stokes, S.M. Loughhead, B.A. Beutel, J.B. Gilbert, K. Nussbaum, A.
1127 Sorrentino, J. Toggweiler, T. Schmidt, G. Gyuelveszi, H. Bernstein, A. Sharei, Cell
1128 engineering with microfluidic squeezing preserves functionality of primary immune
1129 cells in vivo, PNAS. 115 (2018) E10907–E10914.
1130 https://doi.org/10.1073/pnas.1809671115.

1131 [64] R. Xiong, P. Verstraelen, J. Demeester, A.G. Skirtach, J.-P. Timmermans, S.C. De

Smedt, W.H. De Vos, K. Braeckmans, Selective Labeling of Individual Neurons in Dense Cultured Networks with Nanoparticle-enhanced Photoporation, Front. Cell. Neurosci. 12 (2018) 80. https://doi.org/10.3389/FNCEL.2018.00080.

**** Image-guided spatial-selective photoporation through laser beam targeting is demonstrated to allow for selective labeling of individual neurons in dense-cultured networks thereby enabling the study of neuronal morphology.**

[65] X. Huang, A. Pallaoro, G.B. Braun, D.P. Morales, M.O. Ogunyankin, J. Zasadzinski, N.O. Reich, Modular Plasmonic Nanocarriers for Efficient and Targeted Delivery of Cancer-Therapeutic siRNA, Nano Lett. 14 (2014) 2046–2051. https://doi.org/10.1021/nl500214e.

[66] E. Bergeron, C. Boutopoulos, R. Martel, A. Torres, C. Rodriguez, J. Niskanen, J.J. Lebrun, F.M. Winnik, P. Sapieha, M. Meunier, Cell-specific optoporation with near-infrared ultrafast laser and functionalized gold nanoparticles, Nanoscale. 7 (2015) 17836–17847. https://doi.org/10.1039/c5nr05650k.

[67] B. Bošnjak, M. Permanyer, M.K. Sethi, M. Galla, T. Maetzig, D. Heinemann, S. Willenzon, R. Förster, A. Heisterkamp, S. Kalies, CRISPR/Cas9 Genome Editing Using Gold-Nanoparticle-Mediated Laserporation, Adv. Biosyst. 2 (2018) 1700184. https://doi.org/10.1002/adbi.201700184.

[68] J. Liu, T. Hebbrecht, T. Brans, E. Parthoens, S. Lippens, C. Li, H. De Keersmaecker, W.H. De Vos, S.C. De Smedt, R. Boukherroub, J. Gettemans, R. Xiong, K. Braeckmans, Long-term live-cell microscopy with labeled nanobodies delivered by laser-induced photoporation, Nano Res. 13 (2020) 485–495. https://doi.org/10.1007/s12274-020-2633-z.

[69] G.B. Braun, A. Pallaoro, G. Wu, D. Missirlis, J.A. Zasadzinski, M. Tirrell, N.O. Reich, Laser-Activated Gene Silencing via Gold Nanoshell-siRNA Conjugates, ACS Nano. 3 (2009) 2007–2015. https://doi.org/10.1021/nn900469q.

[70] D.P. Morales, W.R. Wonderly, X. Huang, M. McAdams, A.B. Chron, N.O. Reich, Affinity-Based Assembly of Peptides on Plasmonic Nanoparticles Delivered Intracellularly with Light Activated Control, Bioconjug. Chem. 28 (2017) 1816–1820. https://doi.org/10.1021/acs.bioconjchem.7b00276.

1162 [71] D.P. Morales, E.N. Morgan, M. McAdams, A.B. Chron, J.E. Shin, J.A. Zasadzinski,
1163 N.O. Reich, Light-Triggered Genome Editing: Cre Recombinase Mediated Gene
1164 Editing with Near-Infrared Light, Small. 14 (2018) 1800543.
1165 https://doi.org/10.1002/smll.201800543.

1166 [72] X. Li, P. Kang, Z. Chen, S. Lal, L. Zhang, J.J. Gassensmith, Z. Qin, Rock the nucleus:
1167 significantly enhanced nuclear membrane permeability and gene transfection by
1168 plasmonic nanobubble induced nanomechanical transduction, Chem. Commun. 54
1169 (2018) 2479–2482. https://doi.org/10.1039/c7cc09613e.

1170 [73] G. Houthaeve, R. Xiong, J. Robijns, B. Luyckx, Y. Beulque, T. Brans, C. Campsteijn,
1171 S.K. Samal, S. Stremersch, S.C. De Smedt, K. Braeckmans, W.H. De Vos, Targeted
1172 Perturbation of Nuclear Envelope Integrity with Vapor Nanobubble-Mediated
1173 Photoporation, ACS Nano. 12 (2018) 7791–7802.
1174 https://doi.org/10.1021/acsnano.8b01860.

1175 **** This work demonstrates that vapor nanobubble-mediated photoporation can induce**
1176 **reversible nuclear envelope disruption when gold nanoparticles are present in the**
1177 **perinuclear region. The kinetics of these ruptures strongly resemble hallmarks of**
1178 **spontaneous ruptures in laminopathy patient cells thereby offering a valuable tool to**
1179 **study these kinds of pathologies. Both influx and outflux of molecules from the nucleus**
1180 **are demonstrated.**

1181 [74] Y. Pan, S. Neuss, A. Leifert, M. Fischler, F. Wen, U. Simon, G. Schmid, W. Brandau,
1182 W. Jahnen-Dechent, Size-Dependent Cytotoxicity of Gold Nanoparticles, Small. 3
1183 (2007) 1941–1949. https://doi.org/10.1002/smll.200700378.

1184 [75] E. Teirlinck, A. Barras, J. Liu, J.C. Fraire, T. Lajunen, R. Xiong, K. Forier, C. Li, A.
1185 Urtti, R. Boukherroub, S. Szunerits, S.C. De Smedt, T. Coenye, K. Braeckmans,
1186 Exploring light-sensitive nanocarriers for simultaneous triggered antibiotic release and
1187 disruption of biofilms upon generation of laser-induced vapor nanobubbles,
1188 Pharmaceutics. 11 (2019) 201. https://doi.org/10.3390/pharmaceutics11050201.

1189 [76] F. Sauvage, J.C. Fraire, K. Remaut, J. Sebag, K. Peynshaert, M. Harrington, F.J. Van
1190 De Velde, R. Xiong, M.J. Tassignon, T. Brans, K. Braeckmans, S.C. De Smedt,
1191 Photoablation of Human Vitreous Opacities by Light-Induced Vapor Nanobubbles,
1192 ACS Nano. 13 (2019) 8401–8416. https://doi.org/10.1021/acsnano.9b04050.

[77] E.I. Galanzha, Y.A. Menyaev, A.C. Yadem, M. Sarimollaoglu, M.A. Juratli, D.A. Nedosekin, S.R. Foster, A. Jamshidi-Parsian, E.R. Siegel, I. Makhoul, L.F. Hutchins, J.Y. Suen, V.P. Zharov, In vivo liquid biopsy using Cytophone platform for photoacoustic detection of circulating tumor cells in patients with melanoma, Sci. Transl. Med. 11 (2019) eaat5857. https://doi.org/10.1126/scitranslmed.aat5857.